UNIVERSITY OF OKLAHOMA

GRADUATE COLLEGE

PETROPHYSICAL CHARACTERIZATION OF SHALES UTILIZING LABORATORY AND FIELD NMR

A THESIS

SUBMITTED TO THE GRADUATE FACULTY

in partial fulfillment of the requirements for the

Degree of

MASTER OF SCIENCE

By

ALEXANDER BESOV
Norman, Oklahoma
2016

PETROPHYSICAL CHARACTERIZATION OF SHALES UTILIZING LABORATORY AND FIELD NMR

A THESIS APPROVED FOR THE
MEWBOURNE SCHOOL OF PETROLEUM AND GEOLOGICAL ENGINEERING

BY

_____
Dr. Chandra Rai, Chair

_____
Dr. Carl Sondergeld

_____
Dr. Deepak Devegowda

To family, advisor, and friends

Acknowledgements

It has been challenging, yet fun, journey to the completion of this thesis. I have met and learned from many amazing individuals along the way, who will never be forgotten. I could not have completed this work without the guidance and help from my advisors, friends and family.

To my advisors; Dr. Sondergeld and Dr. Rai; thank you for developing my interest in the world of petrophysics way back during my undergraduate years. It is through the generosity of your time and knowledge that I have gained this invaluable experience. Thank you for all of the opportunities that you have opened up for me.

To my closest friends; thank you for making it an amazing two and half years of graduate college experience and for your consistent support: Gabriel Machado, Dana Saeed, Doğa Ecem Şenoğlu and Bryce Hutchinson.

To Ali Tinni, Joe Comisky, Song Dang and the rest of my peers in the IC^3 lab; thank you for the many brainstorming sessions and ideas for improvement of my research. Your contributions had a significant impact on my development as a petrophysicist.

To my shaly sandstone:

> *"Evaluation of petroleum reservoirs is a lot like our dating experiences. We have the conventional sandstones, aka the beautiful ladies that we all want to be with, but they are most likely already being developed. Shales, the complicated females that give you headaches and sleepless nights. We, males, work hard during the optimization and completion of these unconventional resources. In addition, there are carbonates, those are the expensive girls, so unless you got the tools and knowledge for offshore drilling, wait until you make it to Exxon or Shell levels… "*
>
> *Petroleum Dating Guru,*
>
> *Alexander Besov*

Table of Contents

List of Tables

List of Figures

Abstract

Over the years, service companies designed numerous tools for field NMR measurements. Amongst them are CMR-Plus with Schlumberger, MRIL-Prime with Halliburton and MREX with Baker Hughes. NMR logs found success in application to conventional fields, but their application to shales remains a challenge. An impediment to evaluation is due to confinement of fluids to nanometer pores, organic and non-organic porosity, paramagnetic impurities, as well as limitations of the current logging tools. We evaluated applicability of two of these tools in shales with guidance from the results of the laboratory NMR experiments.

Tuscaloosa Marine Shale, TMS, was logged with a CMR-Plus at 200 fph and 350 fph and Woodford Shale with an MRIL-Prime tool. We conducted 1D as well as 2D laboratory NMR experiments on both shales. Tests were performed at the same echo spacing (TE) as the field logging tools, as well as at TE = 0.114 ms. Measurements were obtained on the as received, cleaned, brine imbibed and pressure saturated (5000 psi), dodecane imbibed and pressure saturated (5000 psi) sample states.

NMR measurements in Woodford shale indicate that storage capacity is underestimated by over 55% with echo spacing ranging from 0.6 ms to 0.114 ms. Service companies attempt to compensate for this by applying extrapolation algorithms to TE = 0 ms. However, we show that extrapolation practices should be conducted with caution. In order to tie NMR results between laboratory and field measurements data should be acquired at the same TE values. Additionally, T_2 cutoffs, which are often utilized for the purposes of distinguishing movable and residual fluids, are non-unique and are a strong function of echo spacing. Assuming a T_2 cutoff of 0.8 ms, we show on the TMS samples

that by varying echo spacing from 0.4 ms to 0.114 ms, movable fluid content was overestimated by 45%.

In TMS, mercury injection and NMR results from imbibition and pressure saturation experiments reveal that the pore network is inaccessible to dodecane due to strong affinity for water and high capillary entry pressure. Vertical fractures are apparent in the NGI image log in addition to microfractures observed in the SEM images. Based on the laboratory measurements, it appears that the TMS matrix cannot store hydrocarbons. Unlike other shale plays, hydrocarbons in TMS are likely stored and produced from the microfractures, rather than from organic or inorganic pore system.

Fluids, confined to the nanometer size pores, were investigated with NMR in the early maturity window of Woodford samples. 1D T_2 measurements were not effective in distinguishing brine from low viscosity hydrocarbon (dodecane). T1-T2 signatures of Woodford samples spontaneously imbibed and pressure saturated at 5000 psi with brine and dodecane, as well as NMR response from the non-movable fluids, were obtained with a 2 MHz Oxford-Maran GeoSpec2 spectrometer at TE = 0.114 ms. Samples showed increasing T1/T2 ratio to dodecane following pressurized saturation: dodecane imbibition $T_1/T_2 \geq 5$, dodecane saturation $T_1/T_2 \geq 10$. Small, non-wetting pores are accessed through pressurized saturation, on the order of 4 nm when pressurized with dodecane at 5000 psi. Implications of these finding is such that low viscosity hydrocarbons confined to nanometer size pores experience increasing correlation times or decreasing rotational mobility. Additionally, non-movable hydrocarbons, which remained in the Woodford samples following pressurized cleaning with solvents, showed $T_1/T_2 \geq 30$. Therefore, in

nanometer size pores, T1-T2 signatures of low viscosity hydrocarbons and viscous hydrocarbons are likely to overlap.

Chapter 1: Introduction

Introduction to NMR methods

Nuclear magnetic resonance is becoming a vital tool in the evaluation of unconventional reservoirs. In shales, application of the conventional NMR techniques had limited success and was found to be rather misleading (Kausik et al., 2011; Fleury, 2014). An impediment to evaluation is due to complex relaxation mechanisms in shales, as well as limitations of the current logging tools, such as CMR, MREX or MRIL.

Modern NMR data can be acquired in: longitudinal relaxation (T_1) time, transverse relaxation (T_2) time and a combination of the T_1 and T_2 sequences generating T_1-T_2 maps. Additionally, fluid diffusion coefficients can be calculated with information from multiple echo times (TE) and processed to generate T_2-D maps. Understanding the advantages and limitations of these techniques is essential to characterization of shale reservoirs. This work will focus mainly on the NMR data acquired in shales through T_2 and T_1-T_2 sequences.

T_2 Measurements in Conventional Formations

In conventional reservoirs, measures of total porosity, pore size distribution, permeability and bound fluids are possible through measurements of transverse relaxation times (Timur, 1969; Kenyon, 1992). Due to time consuming measurements of T_1, T_2 data is generally preferred as data acquisition is more time efficient. One dimensional T_2 measurements have been the foundation of NMR evaluation for the last 20 years (Anand et al., 2015). Application of cutoffs based upon lithology allowed for segregation of free-fluid, clay-bound and capillary-bound volumes.

Relaxation mechanisms of fluids in conventional porous media are captured in terms of **Eq.1**. They are bulk relaxation (1st term, $1/T_{2bulk}$), surface relaxation (2nd term, $1/T_{2surface}$) and self-diffusion (3rd term, $1/T_{2diffusion.}$).

$$\frac{1}{T_2} = \frac{1}{T_{2bulk}} + \rho_2 \frac{S}{V} + D\frac{(\gamma * G * TE)^2}{12} \quad \text{..... (1)}$$

Parameters in Eq.1 are defined as follows: ρ_2 is surface relativity, $\frac{S}{V}$ is pore surface to volume ratio; D is the diffusion coefficient of the fluid, γ is the gyromagnetic ratio, G is the magnetic field gradient and TE is the spacing between the CPMG spin echoes.

Hirasaki et al. (2003) describes that in unconfined fluids, bulk relaxation is dominated by intramolecular and intermolecular dipole-dipole interactions, as well as spin rotation. Bulk relaxations of water and light oils are generally around 3000 ms and 1000 ms, respectively. As a result, rocks dominated by large pore bodies or open fractures filled with fluids exhibit relaxation near bulk fluid times, represented by the T_{2bulk} term alone.

The diffusion term in Eq.1 captures information about molecular transport through Brownian motion and/or concentration gradient (Hirasaki et al., 2003). Diffusion complicates the interpretation of transverse relaxation data and diffusion effects can often be minimized by decreasing the echo time (TE) or magnitude of the applied magnetic field. Diffusion can be avoided with the longitudinal T_1 measurements, as they are not affected by diffusion. Additionally, presence of paramagnetic materials and minerals with high magnetic susceptibilities cause local magnetic field gradients, further enhancing relaxation rates (Keating and Rosemary, 2009).

In porous media, Kleinberg (1999) demonstrated that fluid-solid interactions dominate T_1 and T_2 relaxations. Pore surface to volume ratio affects the rate of surface relaxation and

is generally increasing with the complexity of the pore network and clay content. In conventional reservoirs, $\frac{S}{V}$ ratio is often used to convert incremental porosity to distribution of pore sizes.

T_2 Measurements in Unconventional Formations

In unconventional reservoirs, Kausik et al. (2011) describe that porosity is dominated by nanometer size pores, which makes most of the conventional NMR workflows/interpretations inaccurate. Additionally, paramagnetic impurities, presence of organics, gas adsorption and high surface-to-volume ratios in clays and organics all strongly influence relaxation mechanisms in shales (Kausik et al., 2011).

T_2 spectrum obtained in shales does not provide pore size distribution and generally contains very limited petrophysical information as compared to conventional rocks (Fleury, 2014). Erroneous interpretations of T_2 data in shales are due to violation of assumptions used to derive Eq. 1. One assumption is fast diffusion regime, where according to Kleinberg (1999) "the fluid molecules travel the pore several times before being relaxed". Fleury (2014) showed that Eq. 1 is not applicable in shales as "the length scale of the NMR interactions becomes comparable to the pore dimensions (a few nanometers compared to pore thickness of ~ 0.5 nm)".

Recent studies have been focused on NMR responses of fluids in shales, fluid typing, storage capacity and wettability determination (Tinni et al., 2015; Sigal and Odusina, 2011; Nicot et al., 2016; Fleury, 2014; Kausik et al., 2011; Odusina et al, 2011; Sulucarnain et al., 2012; Ozen and Sigal, 2013).

We measured a T_2 response in the early maturity Woodford shale and oil-prone Tuscaloosa Marine Shale (TMS) using a 2 MHz Oxford-Maran GeoSpec spectrometer. Samples were spontaneously imbibed and pressure saturated with dodecane and brine (2.5% KCL) while obtaining data at multiple echo times. Laboratory and field NMR T_2 distributions were compared for fluid content identification. Fluid typing with 1D NMR measurements in shales is challenging, as it is likely for brine and hydrocarbon T_2 spectra to overlap. In addition, evaluation is further complicated by the presence of viscous hydrocarbons and bitumen.

T_1-T_2 Maps: Theory and Applications

T_1/T_2 ratios have been utilized by different authors to characterize fluids in shales by utilizing T_1-T_2 maps (Tinni et al., 2014; Nicot et al., 2016; Fleury, 2014; Ozen and Sigal, 2013). Distinguishing low viscosity and viscid fluids in nanometer size pores remains a challenge as Nicot et al. (2016) found that both fluids are capable of generating high T1/T2 ratios.

Non-movable fluids in shales can be bound to the pore surfaces or stored in inaccessible pores, or can be too viscous to flow. Viscous hydrocarbons and bitumen contribute to non-movable fluids. Bohacs et al. (2013) defines bitumen as soluble in solvents and can be solid or semi-solid with a colloidal structure. Particularly large accumulations of bitumen are present in organic rich shales at the onset of oil generation window. Bohacs et al. (2013) described that organic matter consists of kerogen, bitumen and pyrobitumen. NMR is sensitive to fluid viscosity and is capable of identifying the presence of viscous hydrocarbons (Hirasaki et al., 2003; Bloembergen et al., 1948).

Bloembergen et al. (1948) predicted separation in T_1 and T_2 relaxations with increasing rotational correlation time, τ_c, as displayed in **Figure 1**. τ_c term captures time dependent change in proton orientation and is proportional to fluid viscosity (Hirasaki et al., 2003). In liquids, Hirasaki et al. (2003) attributed efficiency of T_1 build up and T_2 relaxation to molecular tumbling (reorientation of molecules) through intermolecular and intramolecular dipole-dipole interactions. In low viscosity fluids, dipolar magnetic field interactions are minimized due to fast molecular tumbling, prolonging T_2 relaxation and results in T_2 relaxation approaching T_1 (Hirasaki et al., 2003). This concept is known as molecular narrowing. In complex molecular structures, as in bitumen, molecular tumbling is slow and enhanced dipolar field interactions result in more efficient T_2 relaxation, $T_1 >> T_2$.

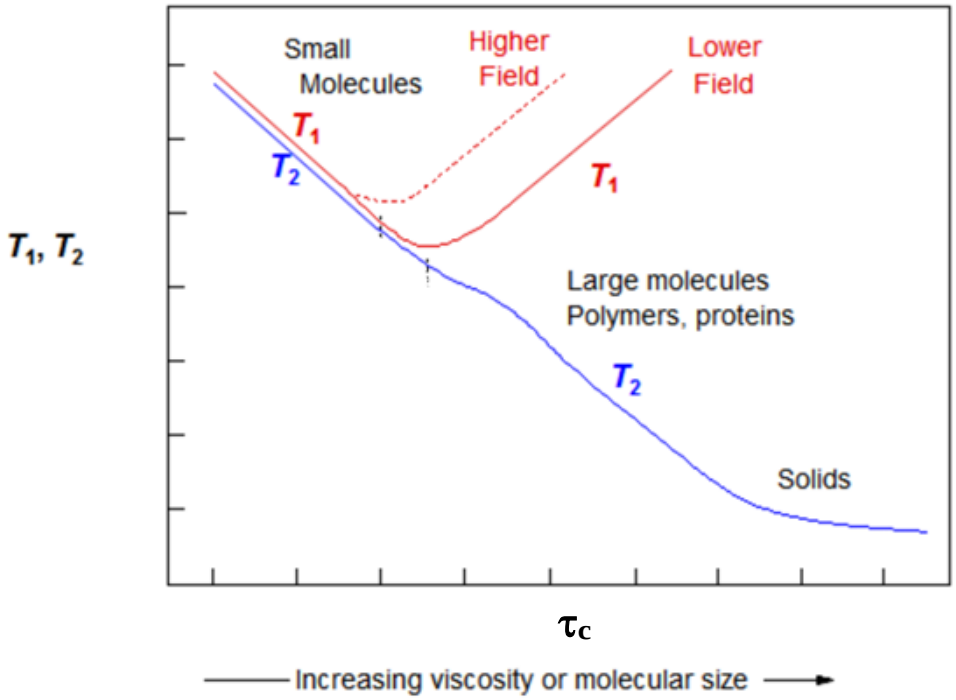

Figure 1— T_1 & T_2 relaxation responses modeled as a function of molecular correlation time, τ_c (modified after Bloembergen et al., 1948).

Fleury (2014) summarized T_1-T_2 responses for various materials in **Figure 2.** He mapped signals from hydroxyls in clays, water and gas in porous media, and bulk fluids. His experiments were conducted at 20 MHz, compared to the 0.5 MHz to 2 MHz field measurements of the logging tools. Additionally, his study did not include signatures of oil or bitumen.

Laboratory T_1-T_2 NMR measurements in this study are conducted at 2 MHz on Woodford and Tuscaloosa Marine shales to further investigate capabilities and limitations of the T_1-T_2 mapping technique in early maturity and peak hydrocarbon generation windows. Samples were imbibed and pressure saturated with dodecane and brine; signatures of non-movable fluids after sample cleaning were also characterized.

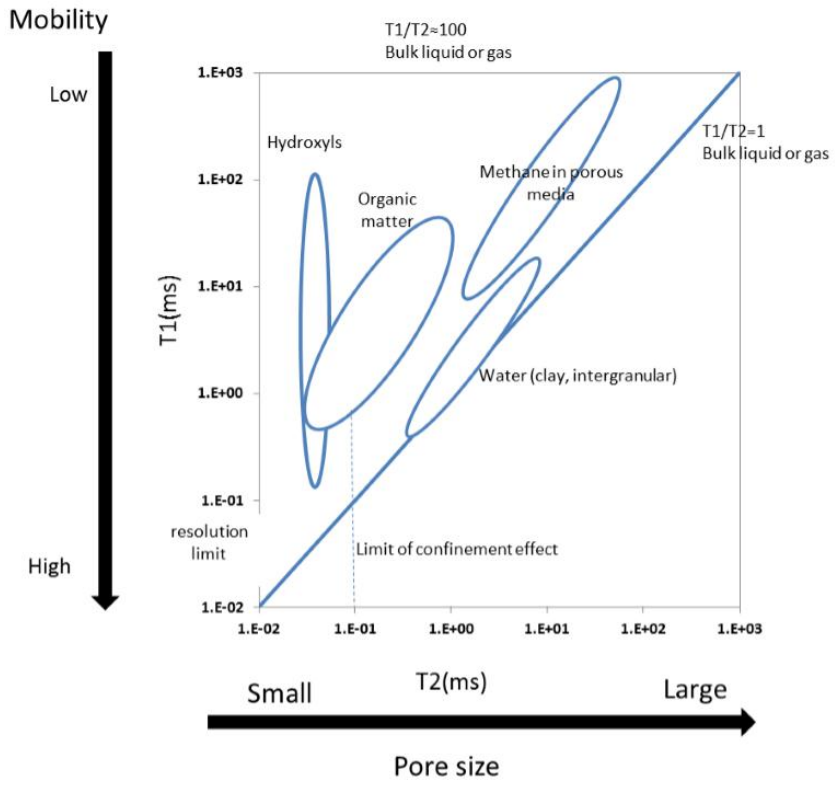

Figure 2— Summary of fluid typing using T_1-T_2 maps (modified after Fleury, 2014).

Chapter 2: NMR Logging Tools

Tool History

First laboratory NMR measurements were made 70 years ago by Block (1946) and Purcell (1946). By 1960, researchers in Chevron proposed field NMR measurements utilizing the Earth's magnetic field for proton polarization. In 1960's, a few service companies started to offer NMR logging services, however, the original measurements did not live up to expectations of the oil and gas industry. First application of the permanent magnets to NMR logging was in 1978 (Kleinberg and Jackson, 2001) to produce an artificial magnetic field which was much stronger than Earth's magnetic field. In 1990, NUMAR successfully tested and announced commercial availability of the MRIL logging services in the field. By 1995, Schlumberger also began NMR measurements in the field with the CMR family of tools. A detailed history on the evolution and developments in the field NMR measurements can be found in Kleinberg and Jackson (2001) and Blumich (2005). Today, numerous service companies apply the principles of magnetic resonance in the field to characterize conventional and unconventional reservoirs. NMR logs found success in application to conventional fields, but their application to shales remains a challenge. Prior to engaging in interpretation of the NMR logs, it is important to understand capabilities and limitations of the modern tools, especially when characterizing mudrocks. Some of the well-known families of tools are CMR (Schlumberger), MRIL (Halliburton) and MREX (Baker Hughes).

Relaxation in shales is a much faster than in conventional reservoir rocks. Older generations of the field NMR tools were not designed to capture signal with very fast relaxation times (nanometer pores). This chapter is focused on exploring the

specifications, operational principles and acquisition sequences of the modern NMR logging tools.

Magnetic Resonance Imaging Log (MRIL) Tool Physics

All modern tools use permanent magnets to polarize protons and apply a radio frequency (RF) pulse to reorient their spin axes. Woodford shale in this study was logged with an MRIL-Prime tool, which is limited to an echo spacing of 0.6 ms. The tool operates at a frequency range of 600-750 kHz; this allows one to obtain multi-frequency measurements as shown in **Figure 3**. High frequency measurements have a shallower cylindrical volume of investigation (10 in. for a 4 ½ in. tool at 200 °F,), while low frequency investigates deeper into formation (11.5 in. for a 4 ½ in. tool at 200 °F). Depending on the diameter of the tool (4 ½ in. or 6 in.), difference between the shallow and the deep radius of investigation ranges from 1.5" to 2". Each frequency generates a cylindrical shell, approximately 1 mm thick (Coates et al, 1999). MRIL-Prime tool can be operated at nine frequencies simultaneously. Static vertical resolution of the tool is two feet. Coates et al. (1999) provide detailed description of the physics of this tool.

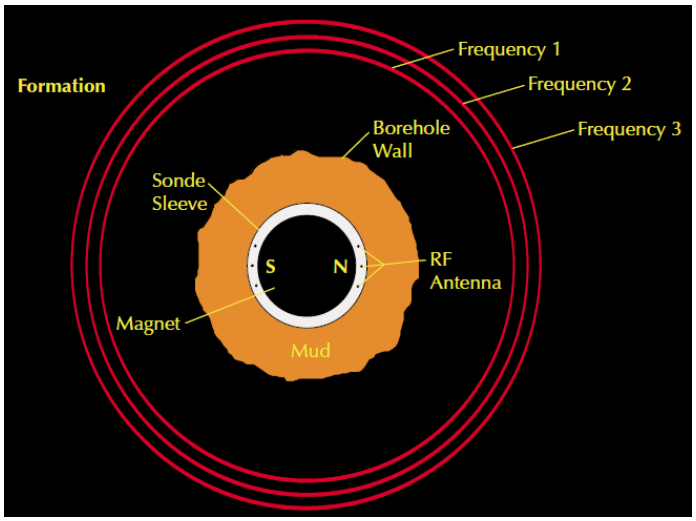

Figure 3— Sensitive regions of investigation generated with multi-frequency (600 - 750 kHz) MRIL measurements (Coates et al., 1999)

Combinable Magnetic Resonance (CMR-Plus) Tools Physics

The CMR-Plus tool is limited to an echo spacing of 0.2 ms. This tool investigates a small volume concentrated around the sensor as displayed in **Figure 4** and has a static vertical resolution of 6 in. CMR-Plus tool is an improvement of the older CMR-200 tool, such that longer permanent magnets (30 in. vs. 12 in.) allow for prepolarization of the protons, and therefore, faster logging rates.

CMR-Plus data is acquired via an Enhanced Precision Mode (EPM) displayed in **Figure 5**. The sequence consists of one long CPMG measurement, followed by a series of short CPMGs, also called bursts (Hook et al., 2011). Hook et al. (2011) showed that bursts improve precision of the porosity measurements in formations with fast relaxation times, such as shales.

CPMG pulse sequences are repeated to acquire data with an opposite phase as shown in Figure 5 to cancel electronic offsets and 180 degree ringing (McKeon et al., 1999). The pair of pulse sequences with opposite phase is called phase-alternated pair (PAP). CPMGs can be programmed to overlap half of the sampling interval to generate “overlapping”

PAP. Phase-alternated pairs can also be obtained "sequentially" by combing CPMG from two nearby sampling intervals (McKeon et al., 1999) eliminating the need for wait time to acquire CPMGs with an alternate phase. Hook et al. (2011) explain that in the CMR software, overlapping PAPs are labeled "CMR-A mode" and sequential PAPs are called "CMR-B mode". CMR-A mode provides better vertical resolution and superior precision over CMR-B mode in fast relaxing porous media; however, this technique under-polarizes fluids with longer T_2 relaxations.

MRIL tool best operates in a moderate conductivity environment. In highly conductive fluids, i.e. brines saturated with salt (sodium ions), performance of the centralized is decreased due to the sodium resonance (Prammer, 2000). According to Prammer (2000) magnetic field gradient of the MRIL tool causes sodium nuclei to resonate. This reduces the signal-to-noise ratio and the logging speed.

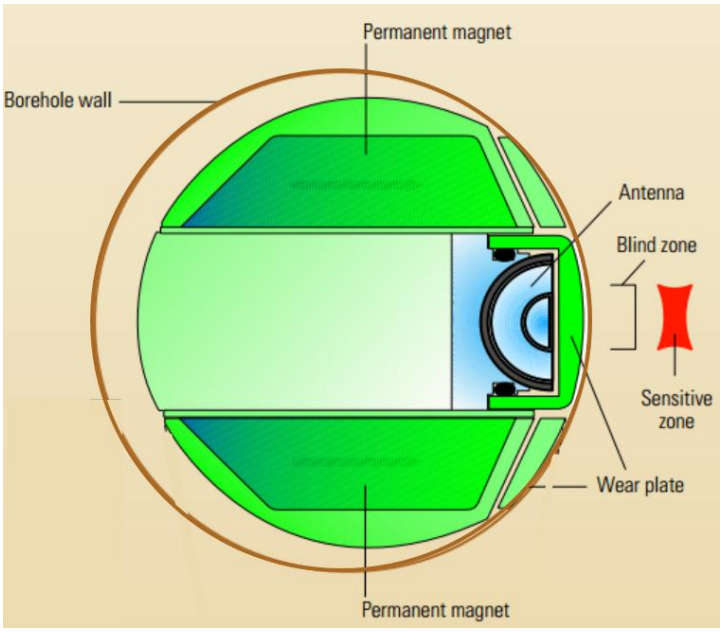

Figure 4—Schematic of the CMR tool showing the concentrated volume of the investigation zone in red (Allen et al., 2000).

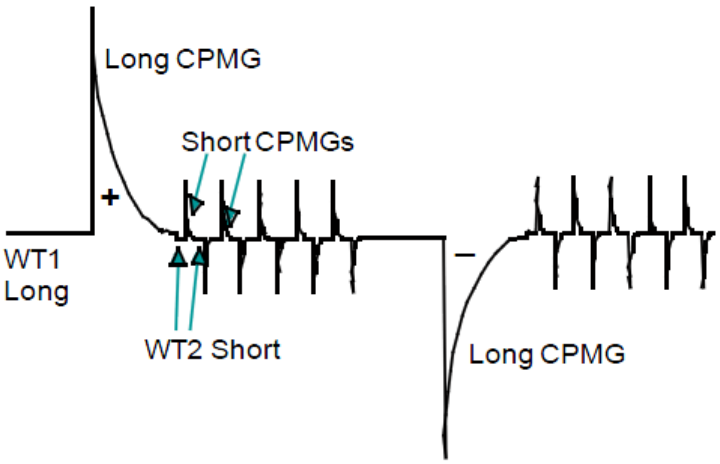

Figure 5—Enhanced Precision Mode, EPM, sequence includes long and short CPMG measurements for improved precision (Hook et al., 2011).

Magnetic Resonance Explorer (MREX) Tool Physics

MREX tool is limited to an echo spacing of 0.3 ms. The tool is eccentered and acquires data over 120 ° region around its sensor as shown in **Figure 6.** Vertical aperture of the tool is 18" and has pre-polarizing magnets above and below the sensor. Tool operates at multiple frequencies (0.5-0.98 MHz) allowing to polarize multiple volumes. Sensitive volume is investigated over 2.1-3.8".

Data acquisition can be customized to various HC types by varying the TE, wait times (TW) and number of echoes (NE). Example of acquisition sequence for medium viscosity oil is show in **Table 1.** A detailed description of the MREX tool and acquisition sequences can be found in Chen et al. (2003).

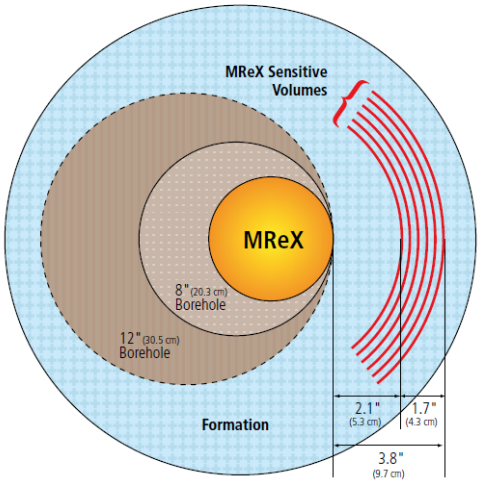

Figure 6— Multi-frequency measurements of the MREX tool generate multiple depth of investigation into formation acquiring data over 120 ° from its sensor (MR Explorer Brochure, 2016a).

Table 1— MREX acquisition parameters for medium viscosity oils (10 to 25 cp) (MR Explorer Brochure, 2016b).

Echo Train(s)	TW (msec)	TE (msec)	NECHO	NREPT	FREQ (kHz)	G (G/cm)	DOI (in)
1A	5100+	2.1	238	1	975	39	2.2
1B	1000	2.1	238	1			
1C	20	0.3	33	12			
2A	5100+	0.6	833	1	870	33	2.5
2B	1000	0.6	833	1			
2C	20	0.3	33	12			
3A	5100+	1.5	333	1	775	28	2.8
3C	20	0.3	33	12			
3D	50	0.4	25	8			
3E	100	0.4	75	4			
3F	200	0.4	125	4			

NMR Logging Tools Summary

Summary of the NMR logging tools from three different vendors are given in **Table 2** and cross-sections of the tools and areas of investigation are shown in **Figure 7**. Their operational frequencies range from 0.5 MHz to 2 MHz. CMR-Plus tool has the best vertical resolution of 6”, while MRIL-Prime averages integrate over 24”. CMR-Plus and MREX are both eccentered tools, while MRIL-Prime is centralized in the borehole.

MRIL-Prime and MREX investigate 360 ° (cylindrical) and 120 ° of the borehole, respectively. CMR-Plus is more effected by borehole rugosity and washouts, as its depth of investigation is just over 1", compared to 3-5" with MRIL-Prime and 2.1-3.8" with MREX. In highly conductive fluids, performance of the centralized MRIL tool is decreased due to the sodium resonance (Prammer, 2000). CMR-Plus and MREX tools are less sensitive to sodium resonance due to the sidewall positioning against the borehole, which minimizes the contribution of +Na from the salt saturated borehole fluids.

Notice that minimum echo spacing (TE) ranges from 0.2 ms to 0.6 ms between the three tools. Raw NMR signals acquired with large echo spacings are insensitive to small pores. CMR-Plus is designed with the shortest echo spacing of 0.2 ms, compared to TE = 0.6 ms in MRIL-Prime and TE = 0.3 ms for MREX tools. Importance of echo spacing in shales is discussed in the "Results and Discussion" chapter.

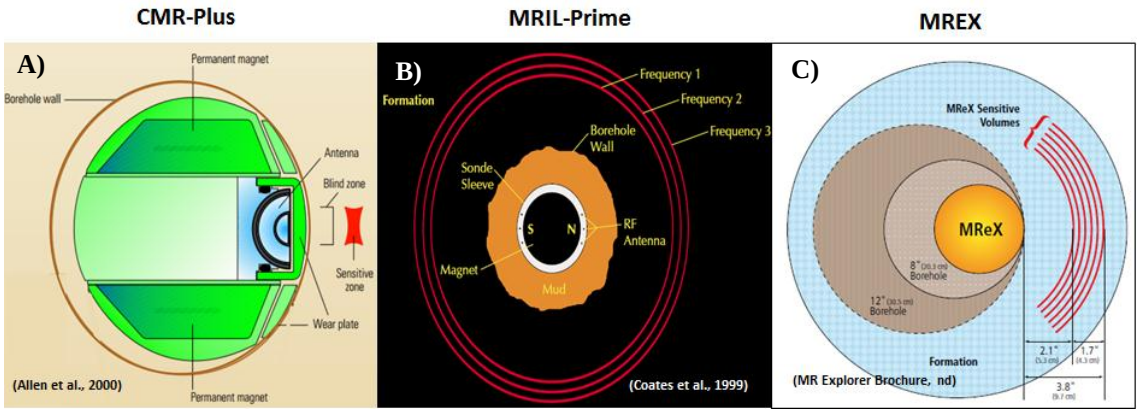

Figure 7—Configurations of the NMR tools offered by service companies: A) CMR-Plus with Schlumberger, B) MRIL-Prime with Halliburton and C) MREX with Baker Hughes.

Table 2— Summary of the three NMR logging tools. * For a 6" tool at 200 °F. Depth of investigation for MRIL-Prime tool 14.5"-16.6"; in a 8.5" borehole the tool investigates 3-5".

	CMR-Plus	MRIL-Prime	MREX
Frequency (MHz)	≈ 2	0.6-0.75	0.5-0.98
Statistic vertical resolution (in.)	6	24	18
Borehole Positioning	Eccentered	Centralized	Eccentered
Degrees of Investigation (°)	few degrees	360	120
Magnetic Field	Constant	Gradient	Gradient
Depth of Investigation (in.)	1.1	14.5-16.5*	2.1-3.8
Sensitivity to Sodium Ions (+Na)	No	Yes	No
Minimum Echo Spacing (TE, ms)	0.2	0.6	0.3

Woodford MRIL Logging Program

MRIL-Prime data was acquired through a Dual Spectra Analysis (DSA) sequence. The equivalent acquisition sequence is displayed in **Figure 8**. It is using a series of Car-Purcell-Meiboom-Gill (CPMG) pulse trains separated by logarithmically spaced wait times (WT). Collections of multiple wait times and inversion of the data provides both T_1 and T_2 distributions (Menger et al., 1999). Time efficient acquisition of multiple wait times is possible with the application of multi-frequency measurements captured in Figure 3.

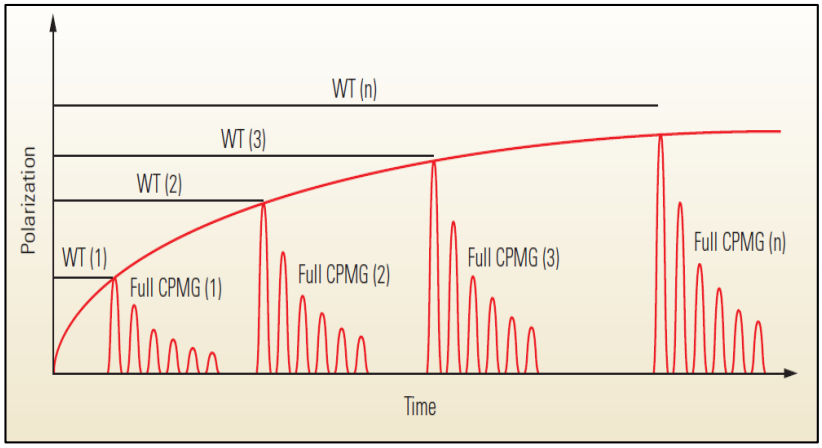

Figure 8— NMR T_1-T_2 acquisition sequence (Akkurt et al., 2009) equivalent to the sequence utilized by an MRIL tool.

Data was processed with Halliburton's in-house activation sets "OKIE" and "T1CVX" as displayed in **Table 3**, further referred to as "Processing 1" and "Processing 2". T_1 build up curve is defined by the number of the WT points. OKIE activation set has a poorly defined T_1 curve at early wait times since fewer wait groups are acquired. The second processing method captures additional information about early decay times since it utilizes more WT points to define the T_1 curve. While we will show later that raw data obtained with an echo spacing of 0.6 ms is too large for characterization of small pores space in shales, fast proton relaxation makes T1CVX activation sequence more applicable to evaluation of unconventional formations compared to the OKIE sequence.

Inversion algorithms involve an assumption of $\Phi_{T1} = \Phi_{T2}$ as observed in **Figure 9**. Note that T_1 and T_2 distributions in the two processing methods are very different from each other. Results from the inversion methods show that reported porosities are within 1 p.u. of each other as observed in **Figure 10**.

Table 3— MRIL data processed using two different activation sets: OKIE and T1CVX.

A) Activation Set OKIE

Group ID	Tw (ms)	TE(ms)	Echoes #
A	8028	1.2	400
B	2130	1.2	400
F	300	0.6	10
E	100	0.6	10
D	30	0.6	10
C	10	0.6	10

B) Activation Set T1CVX

Group ID	Tw (ms)	TE (ms)	Echoes #
A	7000	1.2	600
E	3355	1.2	250
D	1745	1.2	200
B	1250	1.2	150
F	590	1.2	50
I	300	0.6	10
H	100	0.6	10
G	30	0.6	10
C	10	0.6	10

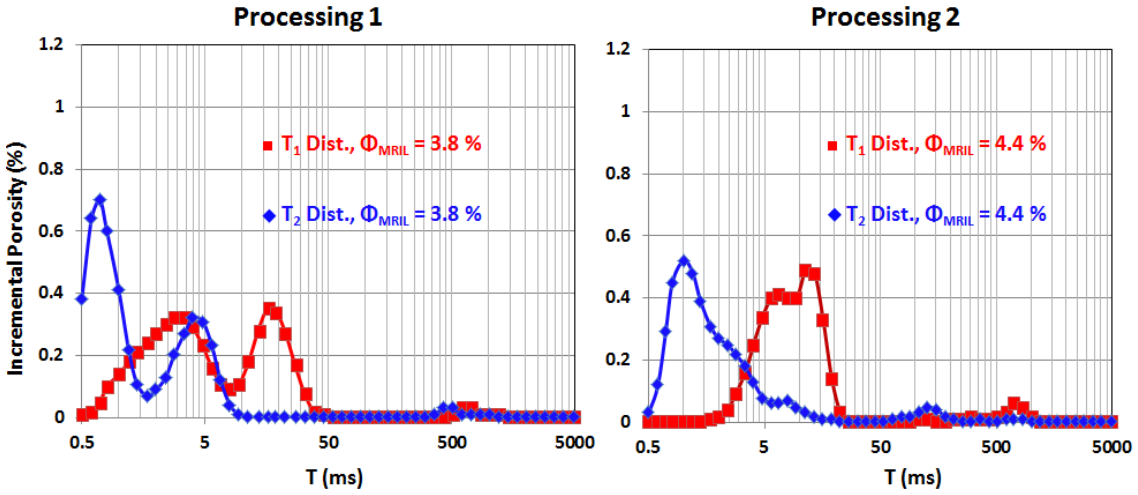

Figure 9— Comparing results of the T_1 and T_2 porosity distributions from the two processing methods at 3875 ft. In spite of the radically different looking spectra, the porosities are the same. T_1 distribution in Processing 1 contains two peak amplitudes, while there is only one peak amplitude in Processing 2.

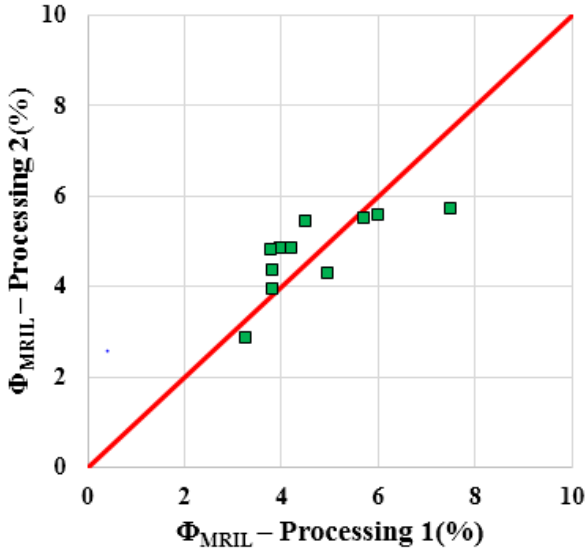

Figure 10—Comparison of porosities from the two processing methods. Displayed points correspond to the depth intervals from which the sidewall core plugs were obtained.

TMS CMR-Plus Logging Program and Data Quality

A total of 24 plugs were extracted from the TMS core (two twin plugs per depth interval) as shown in **Figure 11A**.

The borehole was logged with a CMR-Plus tool. Two logging runs were conducted to investigate the effects of logging speed on SNR and measured porosity, first at 350 fph and second at 200 fph. Data was acquired at an echo spacing of 0.2 ms in CMR-B enhanced precision mode described in the "CMR-Plus Tool Physics" section. The long CPMG sequence was acquired with 5000 echoes and short CPMGs contained 30 echoes. Short CPMG bursts (50 bursts) were obtained following a WT2 of 20 ms. Summary of the parameters to obtain CMR-Plus data for the two logging runs is provided in **Table 4**.

Table 4— Acquisition parameters for the two CMR-Plus logging runs obtained at different logging speeds.

	Pass 1	Pass 2
Logging Speed	350 fph	200 fph
Inter-echo Spacing	0.20 ms	0.20 ms
WT 1 Echoes	5000	5000
WT 2 Echoes	30	30
WT 2 Polarization Time	20 ms	20 ms
# Bursts	50	50
Uphole Stacking	3	3
Average SNR	6.8	7.0

Comparison of the CMR spectra from both logging runs (see **Figure 11**) reveals on average more signal is present at relaxation times above 10 ms in the T_2 spectrum of the 200 fph logging run. Possible explanations for this could be due to design of the CMR-Plus tool or due to underpolarization of fluids if the formation was logged too fast; this is investigated in the "Results and Discussion" sections. CMR-Plus tool is designed with a narrow focus (DePavia et al., 2003) and if the sensor is oriented in the same direction with a fluid filled vertical fractures, longer relaxation times become more apparent.

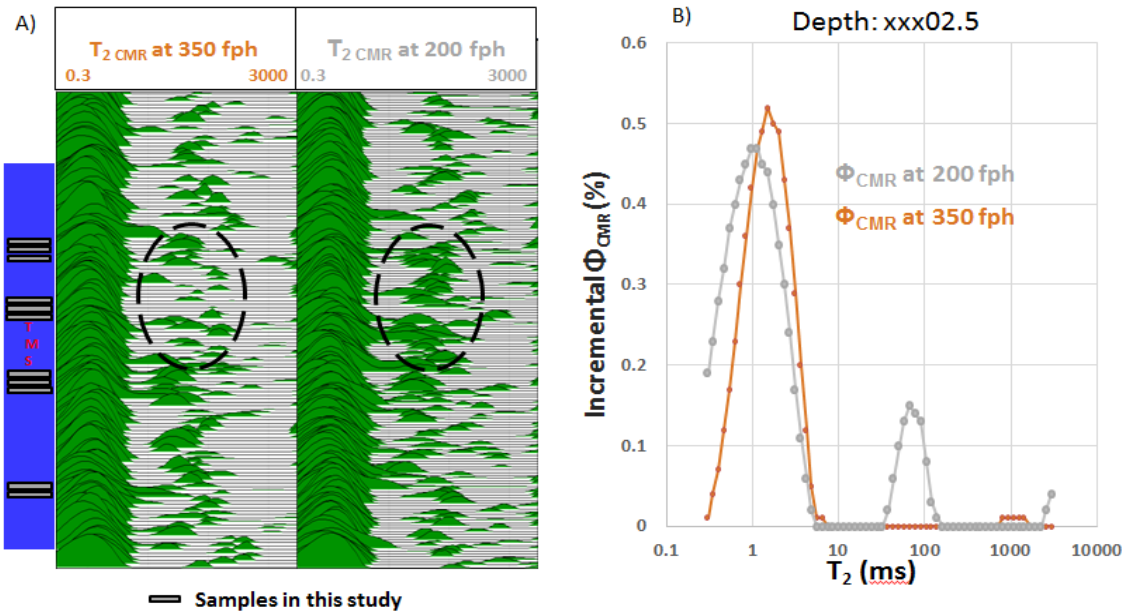

Figure 11—A) Samples selected for this study are shown in the first track (blue). Formation was logged twice with a CMR-Plus tool at 200 fph and 350 fph. B) Additional signal is observed in the T_2 spectra of the slower logging run above 10ms.

CMR-Plus porosity and signal-to-noise ratio (SNR) measured in the wellbore are displayed in **Figure 12**. SNR captures the quality of NMR data, as a ratio of the "initial magnetization amplitude in echo train data to the average noise amplitude" (Saidian, 2015). The borehole is well conditioned as shown in the caliper log in track 1 (Figure 12) and did not affect the quality of the raw CMR measurements. Average SNR is 6.8 and 7.0 for the faster and slower logging runs, respectively.

Cross-plot comparing CMR porosities measured with the two logging runs is shown in **Figure 13**. Reported porosities are within 2 p.u. of each other. Mean porosity for the faster and slower logging run is 6.9% ± 0.9 std. and 7.0% ± 0.7 std., respectively. Uncertainty of 2 p.u. in a 7 p.u. rock produces an error of 28%.

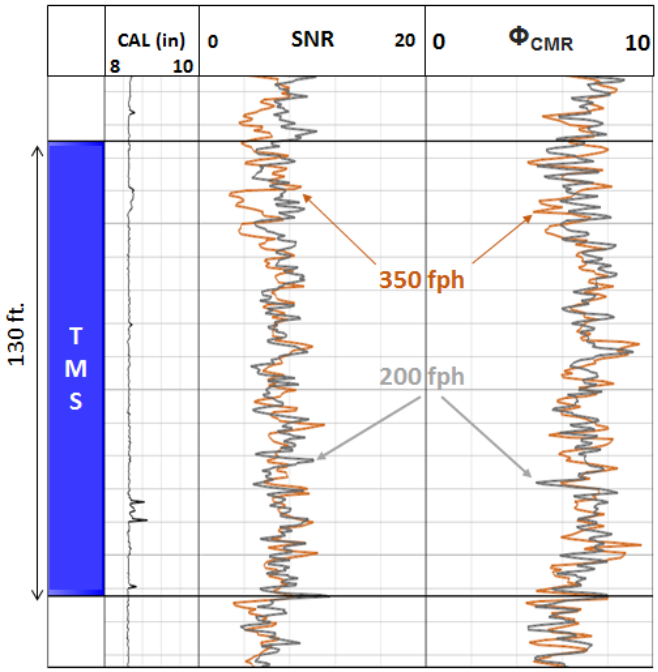

Figure 12—Effects of SNR and borehole quality on the porosity obtained from the CMR-Plus tool.

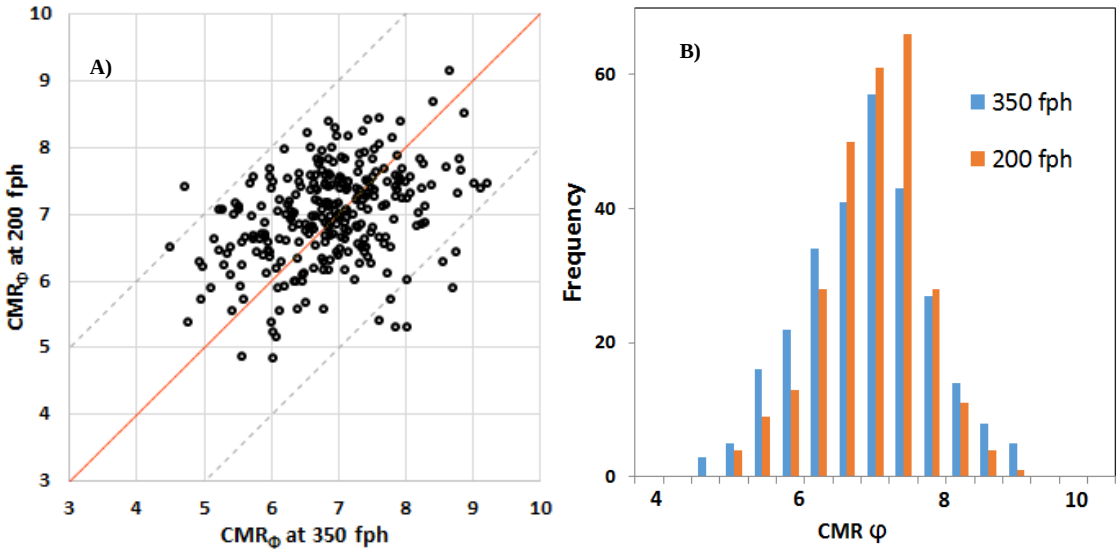

Figure 13—Comparison of the measured CMR-Plus porosities: A) Cross-plot of porosities for the two logging speeds; reported porosities are within 2 p.u. of each other. Uncertainty of 2 p.u. in a 7 p.u. rock produces an error of 28%. B) Histogram of porosities for the two logging speeds (350 fph: mean ϕ = 6.9% ± 0.9 std.; 200 fph: mean ϕ = 7.0% ± 0.7 std.)

Chapter 3: Geology and Sample Description

Tuscaloosa Marine Shale Geology

The Tuscaloosa Marine Shale (TMS) formation, deposited during the Upper Cretaceous, extends from Louisiana to the Southern portion of Mississippi as in **Figure 14A**. The Tuscaloosa Marine Shale is a part of the Tuscaloosa group, consisting of three units: Upper Tuscaloosa, Marine Shale and Lower Tuscaloosa **(Figure 14B)**. Mancini and Puckett (1987) described the TMS as "dark gray, silty, micaceous, fossiliferous, calcareous mudstone". Lower Tuscaloosa consists of coarse-grained sand and lenticular sand/shale intervals deposited in the fluvial-deltaic environment (Lu et al., 2015; Howe, 1962). TMS is overlaid by fluvial Upper Tuscaloosa deposited during regressive infilling (Mancini and Puckett, 2005; Lu et al., 2015). The geochemical studies conducted by Echols et al. (1997) revealed that TMS sourced the Lower Tuscaloosa sands.

Since 2012, TMS has become an active target for hydrocarbon production. Several wells producing from the TMS had an initial production larger than 1000 bbl/day (Anderson 18H-1, Encana; Crosby 12-1H, Goodrich; Weyerhaeuser 73H-1, Encana) (Sanchez Energy, 2015). This makes the TMS an attractive unconventional shale play. Despite the fact that the TMS produces considerable amounts of hydrocarbon, the true potential and the factors controlling the production of hydrocarbon remain elusive. Previous studies have been conducted in attempts to understand structure, stratigraphy and resource potential of the Tuscaloosa Marine Shale (John et al., 1997; Lu et al., 2015; Allen et al., 2014). John et al. (1997) delineated the extent, depth as well as the thickness of the TMS. They estimated the amount of hydrocarbon stored in the TMS to be close to of 7 billion barrels of oil, assuming 50 barrels of oil per acre-foot. Allen et al. (2014) determined

hydrocarbon distribution of TMS by mapping elevated resistivity in southwestern Mississippi and concluded that elevated resistivity is attributed to matured oil-prone sections of TMS. Lu et al. (2015) investigated the impact of porosity, organic matter and mineralogy on the resistivity values observed in the TMS and concluded that organic matter (TOC) was the main factor controlling the variability in the resistivity values.

In this study, TMS was evaluated with laboratory and field NMR to understand the hydrocarbon storage and the factors controlling production of hydrocarbons.

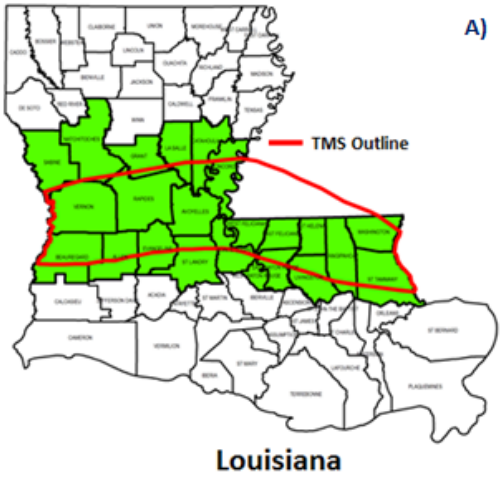

CRETACEOUS	GULF	SELMA	SELMA CHALK (UNDIFF.)	CHALK B)
		EUTAW	EUTAW (EAGLEFORD)	GRAY SHALE AND BASAL SAND
		TUSCALOOSA	UPPER TUSCALOOSA	SANDS AND SHALES
			MARINE SHALE	DARK GRAY MARINE SHALE
			LOWER TUSCALOOSA STRINGER MASSIVE SAND	LENTICULAR SANDS AND SHALES WHITE, COARSE-GRAINED
	COMANCHE	WASHITA-FREDSBG.	DANTZLER	SANDS AND SHALES
			UNDIFFERENTIATED	PREDOMINANTLY LIMESTONE
		TRINITY	PALUXY	VARIABLY COLORED SANDS AND SHALES

Figure 14—A) Map showing outline of TMS in Louisiana and Mississippi (State of Louisiana Department of Natural Resources, NA) B) Stratigraphy (modified after John et al., 2005)

TMS Petrophyisical Properties

Results of the petrophysical measurements on the 12 samples are shown in **Table 5**. Mineralogy was measured through transmission Fourier Transform Infrared Spectroscopy (FTIR) (Sondergeld and Rai, 1993; Ballard, 2007). Formation is dominated by clays, averaging 63 ± 14 wt%, where illite and mixed-layer clays are the prevailing clay minerals at 47 wt% and 28 wt%, respectively. Smectite content was 7 wt%, which could be a concern for drilling and completion operations. Average calcite, quartz and

feldspar contents are 11 wt%, 7 wt% and 8 wt%, respectively. Total clays and calcite are the only minerals that show a considerable dynamic range within one standard deviation. Measured LECO™ TOC content for 12 samples is 1.6 ± 0.6 wt%, with a range from 0.4 to 2.3 wt%. Average crushed helium porosity is 5.5 ± 0.9%, with a range from 3.7% to 6.6%. Helium porosity results are lower compared to the laboratory brine saturated NMR measurements as will be shown in the "Results and Discussion" section. Helium porosity does not distinguish organic from inorganic porosity, however results from the SEM images show that a majority of TOC is not porous and appears to have flowed as observed in **Figure 15**. SEM images were obtained on ion milled surfaces using an FEI Helios 600 Dual-Beam FIB/SEM in back-scattered electron (BSE) mode. Dark areas in the image are representative of the organic matter while the lighter colors represent inorganic matrix minerals. As observed in the SEM images, samples also contain numerous microcracks which might contribute to hydrocarbon production.

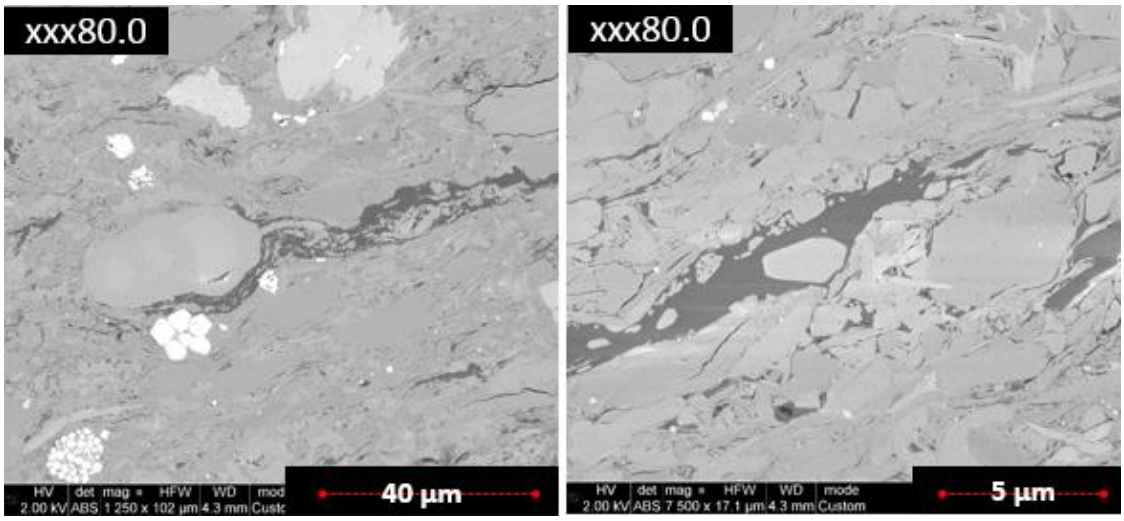

Figure 15—SEM images of broad beam ion milled TMS surfaces operated in BSE mode reveal that organic porosity is negligible. Dark areas in the image are representative of the organic matter while the lighter colors are capturing inorganic matrix minerals. TOC is not porous and appears to have a flow structure.

Table 5—Summary of routine petrophysical measurements in TMS

	Sample	xxx 86.7	xxx 89.2	xxx 91	xxx 34.5	xxx 35	xxx 40.4	xxx 75.5	xxx 76.6	xxx 79.5	xxx 11.4	xxx 12.2	xxx 14.8
Mineralogy (wt.%)	Mixed Clays	21.1	15.4	5.0	6.7	24.0	19.3	17.6	11.5	29.8	8.7	27.2	26.8
	Illite	26.5	29.5	32.7	10.2	19.4	33.7	31.8	51.3	34.4	34.7	29.1	20.2
	Smectite	4.0	3.5	14.2	0.0	1.6	6.8	2.3	6.6	4.7	1.6	1.4	5.1
	Kaolinite	8.2	9.5	12.5	5.3	9.4	12.6	7.2	9.3	8.3	12.6	12.0	11.5
	Quartz	25.8	9.7	8.4	5.8	1.1	9.7	9.2	3.3	4.1	5.7	1.9	0.0
	Calcite	5.6	17.6	1.9	53.9	32.6	0.0	7.1	0.0	1.1	12.3	5.6	0.0
	Total Feldspars	6.8	6.6	8.8	4.1	8.0	8.5	5.9	5.9	6.1	11.2	7.9	18.1
	Siderite	2.0	6.3	8.2	9.1	3.0	6.3	10.1	8.1	7.6	8.6	9.6	10.0
	Apatite	0.0	1.5	1.3	2.2	0.8	1.9	1.4	1.7	1.0	4.6	4.8	1.4
	Quartz	25.8	9.7	8.4	5.8	1.1	9.7	9.2	3.3	4.1	5.7	1.9	0.0
	Pyrite	0.0	0.0	7.1	0.0	0.0	0.0	0.0	0.0	0.0	0.0	0.0	4.1
	Leco TOC (wt%)	1.0	1.3	0.9	2.0	2.2	0.4	2.2	2.2	2.3	1.9	1.4	1.4
SRA	S1 (mg/g)	0.6	0.4	0.5	1.4	1.0	0.3	1.2	1.0	1.1	x	x	x
	S2 (mg/g)	2.1	1.0	1.6	4.7	3.3	0.5	4.9	4.5	5.6	x	x	x
	Tmax (°C)	444.6	442.6	444.2	445.6	444.9	441.3	446.3	447.2	445.5	x	x	x
	S3 (mg/g)	0.2	0.1	0.1	0.3	0.2	0.0	0.2	0.1	0.3	x	x	x
	HI	122.0	84.0	104.0	188.0	147.0	67.0	180.0	183.0	210.0	x	x	x
	OI	9.0	8.0	9.0	11.0	11.0	6.0	7.0	5.0	13.0	x	x	x
	PI	0.2	0.3	0.2	0.2	0.2	0.4	0.2	0.2	0.2	x	x	x
	*Ro calc (%)	0.84	0.81	0.84	0.86	0.85	0.78	0.87	x	0.86	x	x	x
Crushed	RHOB (gm/cc)	2.60	2.60	2.59	2.58	2.57	2.61	2.55	2.56	2.56	2.58	2.59	2.59
	Crushed helium grain density (gm/cc)	2.71	2.71	2.72	2.66	2.67	2.75	2.66	2.69	2.70	2.67	2.69	2.71
	Crushed helium Φ (%)	5.2	5.6	6.3	3.7	4.5	6.6	6.1	6.0	6.2	4.3	4.6	5.2

* Ro_{calc} (%) is calculated from Jarvie et al. (2001):$Ro_{calc} = 0.018 * Tmax - 7.16$

Woodford Shale Geology

Late Devonian to Early Mississippian Woodford Shale has been a major source of hydrocarbons in Oklahoma; it was deposited during a global sea-level transgression (Johnson, 1988). Guo et al. (2010) describe Woodford Shale as organic-rich, fissile black shale deposited in highly anoxic conditions, making it a valuable petroleum source rock. Samples in this study are from the Arkoma Basin, which extends across South-Eastern Oklahoma as shown in **Figure 16**. Viele and Thomas (1989) describe formation of the Arkoma basin due to crustal loading during Ouachita orogeny. Generally, the basin is known for being thermally overmature, caused by high heat flow, hydrothermal fluid flow, stratigraphic and structural burial (Houseknecht et al., 2014; Houseknecht and Matthews, 1985; Houseknecht et al., 1992; Cardott, 2001, 2013). Cardott (2012) mapped vitrinite reflectance (VR) and identified areas over 6% Ro in the eastern flank of the basin as displayed in **Figure 17**. VR decreases below 1% in the western basin margin where the core plugs have been obtained in this study.

Over 1000 wells have been drilled through the Woodford Shale (Houseknecht et al., 2014) in the Arkoma Basin. Most of these wells are focused in the condensate to dry gas maturity window. Recent exploration efforts have been attempted in the shallower oil bearing sections of this play. High structural dip and abrupt change in elevation create challenging conditions for economic hydrocarbon production. One of the major challenges with drilling economic wells at the onset of oil generation window is distinguishing movable from non-movable hydrocarbons. Non-movable hydrocarbons are associated with long chain molecules too viscous to be mobile.

This study investigates application of NMR in distinguishing movable and non-movable fluids, as well as to perform fluid typing in the Woodford Shale.

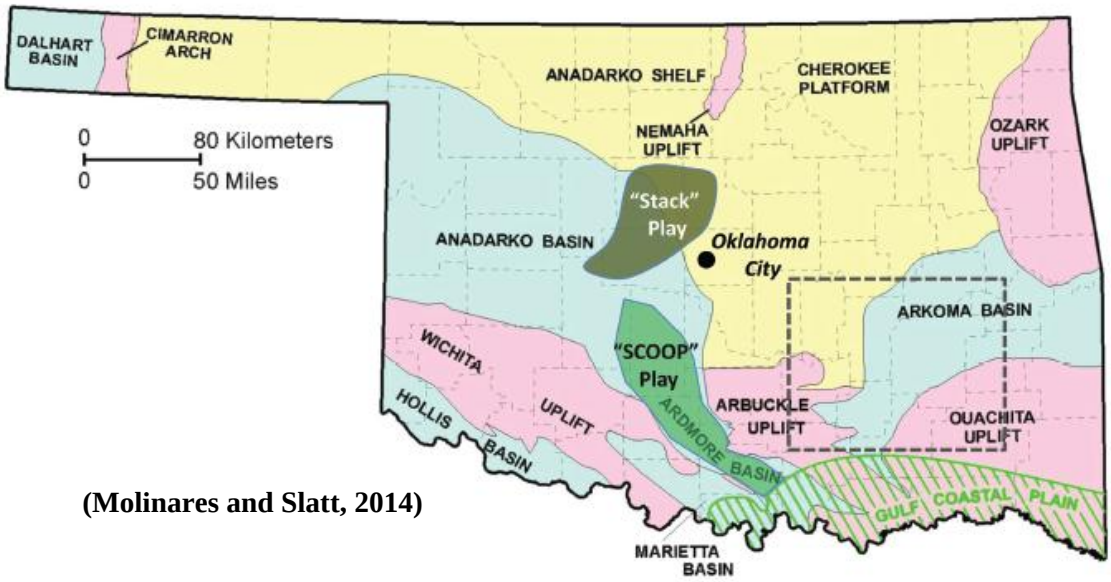

(Molinares and Slatt, 2014)

Figure 16— Arkoma Basin is enclosed between the Cherokee platform and Ozark uplift in the North, Ouachita Uplift and Arbuckle Uplift in the South (after Molinales and Slatt, 2014).

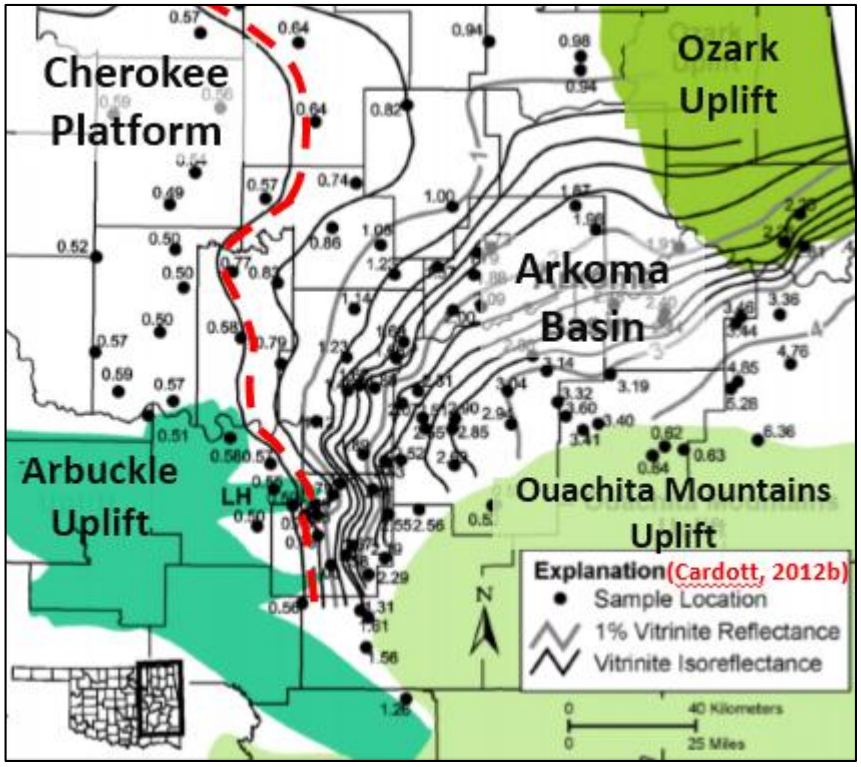

Figure 17— Vitrinite reflectance map generated for Arkoma Basin (Cardott, 2012). Location of the well cannot be revealed, however, it is along the red isoreflectance line of 0.6%.

Woodford Shale Petrophysical Properties

A total of 10 rotary sidewall plugs were cored with a water based mud. Summary of the measured petrophysical properties are provided in **Table 6.** Mineralogy was measured through transmission Fourier Transform Infrared Spectroscopy (FTIR). The formation is dominated by clays, quartz and feldspars at 41±9 wt.%, 39±12.8 wt.% and 10±5 wt.%, respectively. Prevailing clay minerals are illite and mixed-layer clays at 65 wt.% and 34 wt.%. Calcite and dolomite contents are negligible, while average siderite contribution is 5 wt.%.

Measured LECO™ TOC content on 10 samples is 7.1±2.2 wt.%, indicating an excellent source rock potential. Storage capacity is low in this section of Woodford as the measured average crushed helium porosity is 3.4 ± 0.4%, with a range from 3.0% to 4.3%. Thermal

maturity estimated from SRA Tmax data indicate that these samples are currently at the onset of oil generation window, averaging $Ro_{\_tmax}$ = 0.75 %. Average measured vitrinite reflectance on one of the samples is 0.6% as displayed in **Figure 18**. Samples with low maturities typically do not have organic porosity (Curtis et al., 2012), as evidenced in SEM images of samples 3957, 3913 and 3863 in **Figure 19**. SEM images were obtained on broad beam argon ion milled surfaces using an FEI Helios 600 Dual-Beam FIB/SEM in back-scattered electrons (BSE) mode, where dark areas are representative of organic matter and lighter colors show inorganic matrix.

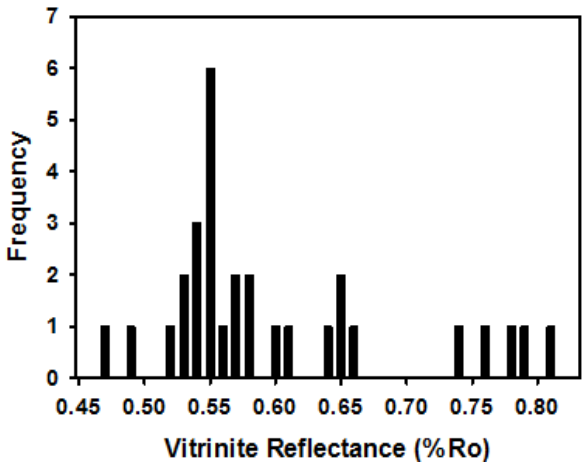

Figure 18— Vitrinite reflectance measured on one of the samples from this study by Cardott, 2015 (personal communication). After 30 vitrinite measurements, average R_0 = 0.6% ± 0.1% std.

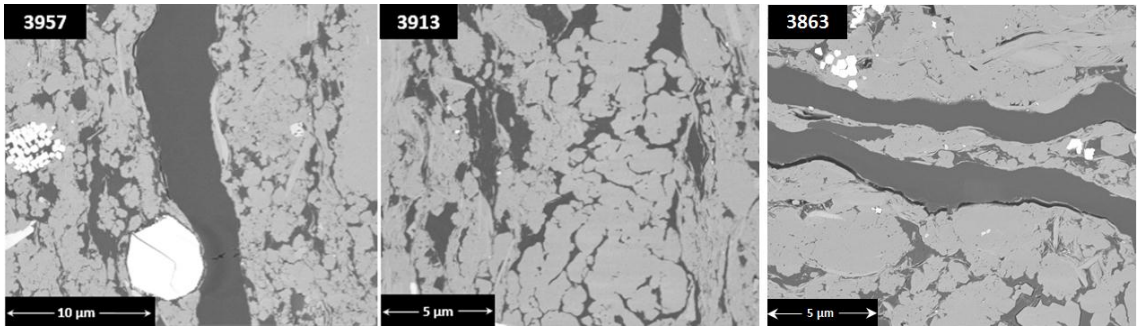

Figure 19 — SEM images of ion milled Woodford surfaces generated in BSE mode. Samples 3957, 3913 and 3863 show no organic porosity.

Table 6—Summary of the petrophysical measurements in Woodford Shale

	Sample	3863	3863.2	3875	3879	3883	3906	3913	3917	3951	3957
Mineralogy (wt.%)	Mixed Clays	0.0	12.9	10.5	6.6	16.9	18.6	20.7	14.8	9.4	22.4
	Illite	37.0	21.3	23.9	36.6	19.2	23.4	20.2	17.9	38.2	11.1
	Quartz	38.2	46.9	46.8	34.5	46.8	34.6	48.1	48.3	21.1	52.4
	Calcite	0.0	0.0	0.0	0.0	0.0	0.0	0.0	0.0	0.0	0.0
	Dolomite	0.0	0.0	0.0	0.0	0.0	6.0	0.0	0.0	0.0	0.8
	Pyrite	0.0	0.0	0.0	18.4	0.0	0.0	0.0	0.0	0.0	0.0
	Total Feldspars	10.9	10.1	6.4	2.3	7.5	10.4	5.0	12.3	22.5	3.9
	Anhydrite	2.0	0.0	0.5	0.0	0.7	0.9	0.0	1.1	1.7	1.4
	Siderite	9.2	6.1	7.8	1.5	7.1	4.4	2.9	4.4	1.9	4.9
	Aragonite	2.6	2.6	1.6	0.0	1.7	1.6	3.1	0.5	2.2	3.0
	LECO TOC (wt%)	6.4	5.5	8.0	6.5	7.3	7.3	6.5	9.2	10.4	9.9
SRA	S1 (mg/g)	4.2	5.2	6.7	3.8	5.5	4.5	4.2	6.6	4.6	6.0
	S2 (mg/g)	28.3	40.0	57.2	42.3	50.7	44.5	44.8	77.3	80.3	71.4
	Tmax (°C)	438.3	437.4	437.8	437	439.8	441.5	438.9	442.1	436.7	438.6
	S3 (mg/g)	0.1	0.1	0.2	0.4	0.5	0.6	0.7	0.9	1.3	1.4
	HI	410	518	579	483	562	561	550	664	663	636
	OI	1	1	2	5	6	7	9	8	10	12
	PI	0.13	0.11	0.1	0.08	0.1	0.09	0.09	0.08	0.05	0.08
	* Ro calc (%)	0.73	0.71	0.72	0.71	0.76	0.79	0.74	0.80	0.70	0.73
Crushed	RHOB (gm/cc)	2.30	x	2.53	2.35	2.31	2.33	2.34	2.26	2.19	2.21
	Crushed Helium grain density (gm/cc)	2.39	x	2.61	2.43	2.38	2.40	2.40	2.33	2.27	2.27
	Crushed Helium Φ (%)	4.4	x	3.3	3.7	3.5	3.5	3.3	4.0	3.9	3.1

*Ro_{calc} (%) is calculated from Jarvie et al. (2001):$Ro_{calc} = 0.018 * Tmax - 7.16$

Chapter 4: Experimental Procedures

Pressurized Solvent Extraction

Woodford shale samples were cleaned with a Buchi SpeedExtractor™. Samples were cleaned in three cycles (total duration of 5 hours) with an 80/20 toluene and methanol mixture at a 100 ^{o}C and a pressure of 1500 psi. Woodford samples contained significant bitumen content as shown in **Table 6** and sample cleaning was needed to characterize the pore space occupied by viscid organics. TMS samples were not cleaned with solvents in any of the experiments in this study.

Laboratory NMR Acquisition Sequences

T_2 and T_1-T_2 measurements were conducted on Woodford Shale and TMS with an Oxford GeoSpec2™ instrument operating at 2 MHz. Data was obtained on 10 Woodford samples (Arkoma Basin) and 24 Tuscaloosa Marine Shale (TMS) samples (12 twin plugs). Core plugs dimensions were 1.0" in diameter and 2.0" to 2.5" in length. Shales were imbibed and pressurized at 5000 psi with dodecane and brine (25,000 ppm KCl).

T_2 data was obtained through the Car-Purcell-Meiboom-Gill (CPMG) pulse sequence shown in **Figure 20**. Time delay between the echoes is known as echo time (TE, TE = 2 * Tau). A 90° rf pulse orients protons in the x-y plane, while consecutive 180° pulses generate "Hahn's Echoes" (Hahn, 1950). Depending on the sample, complete polarization was achieved with recycle delays ranging from 0.5 sec to 1.5 sec, generating CPMG pulse sequences ranging from 1250 to 5000 echoes. Data was acquired with a signal-to-noise ratio (SNR) range of 30-100.

T_1 measurements were not performed, however, T_1 sequence is described to explain acquisition of the T_1-T_2 maps. T_1 sequence shown in **Figure 21** is known as "inversion recovery" and consists of a 180° pulse, followed by 90° pulse to record a Ti point. Time periods between 180° and 90° pulses are varied to obtain multiple Ti points. Ti points are spaced logarithmically and constitute the T_1 build up data.

T_1-T_2 data is acquired through an inversion recovery CPMG pulse sequence displayed in **Figure 22**, which is a combination of the T_1 and T_2 pulse sequences. Sequence begins with an inversion recovery sequence to obtain a Ti point, followed by a CPMG sequence recording transverse relaxation decay. Sequence is repeated for a range of Ti values to generate 2D T_1-T_2 maps.

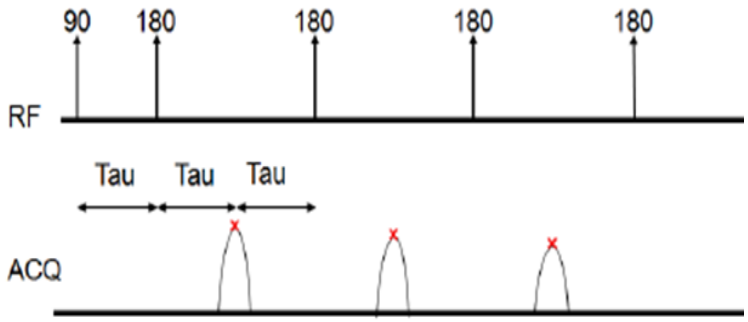

Figure 20— CPMG pulse sequence to obtain T_2 NMR data (Green Imaging Technologies, 2014).

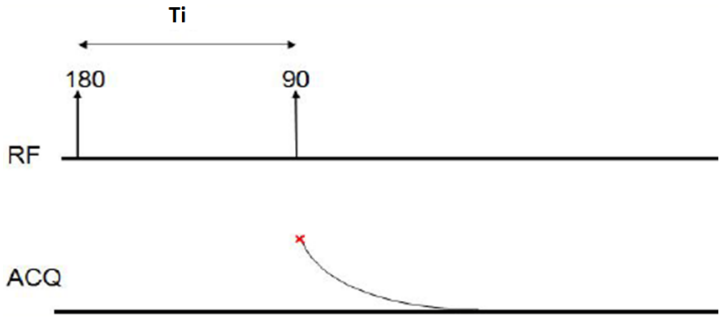

Figure 21—Inversion recovery pulse sequence for T_1 data acquisition (Green Imaging Technologies, 2014).

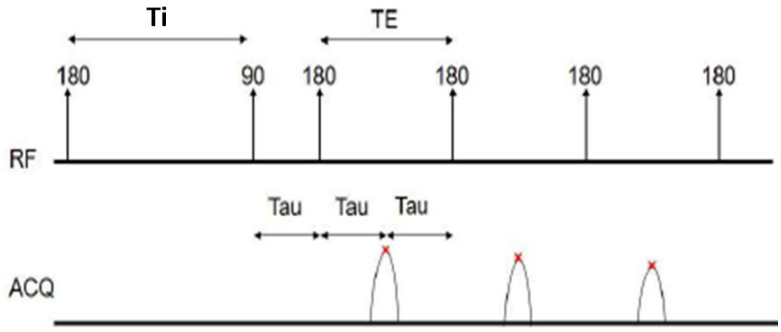

Figure 22— Inversion recovery CPMG pulse sequence to obtain T_1-T_2 data (Green Imaging Technologies, 2014).

Laboratory NMR Experimental Procedure and Measurements

Tuscaloosa Marine Shale

Twin plugs were obtained to conduct independent NMR measurements with brine and dodecane on the "as received" plugs. Procedure for the measurements is outlined in **Figure 23**. An NMR T_2 spectrum was first acquired on the "as received" plugs, followed by parallel imbibition with dodecane and 2.5% KCl brine for 48 hours. Samples fractured during imbibition with brine. NMR response was acquired on the fractured plugs. Measurements were conducted at the echo spacing of 0.2 ms and 0.114 ms. For comparison of laboratory and field data, laboratory measurements were conducted at the same TE as the CMR-Plus tool (0.2 ms). In addition, T_1-T_2 NMR maps were collected at an echo spacing of 0.114 ms on the "as received" and brine imbibed samples.

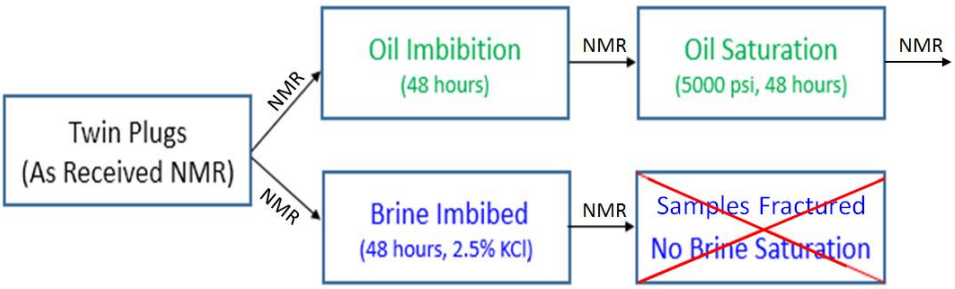

Figure 23— Laboratory NMR procedure used to imbibe and saturate twin plugs with oil and brine.

Woodford Shale

Woodford plugs were obtained by rotary sidewall coring using water based mud. NMR experiments were conducted in series of steps shown in **Figure 24** using TE = 0.114 ms and 1.2 ms. Data acquired with larger echo spacing was compared to the results from the MRIL logging tool operating at the same TE. Samples were cleaned with SpeedExtractor E-916 in three cycles at a 100 ^{o}C and a pressure of 1500 psi using an 80/20 toluene/methanol mixture. After cleaning, samples were spontaneously imbibed with dodecane for 48 hours. NMR signal was acquired following imbibition. Samples were then pressurized (5000 psi) with dodecane for 48 hours and new NMR signal was obtained. Prior to imbibing and saturating samples with a 2.5 % KCl brine, they were airdried and vacuumed to mitigate signal contribution from dodecane. NMR signal was acquired after each of the imbibition/saturation experiment as shown in Figure 24. Pressurized brine saturation was conducted at 5000 psi.

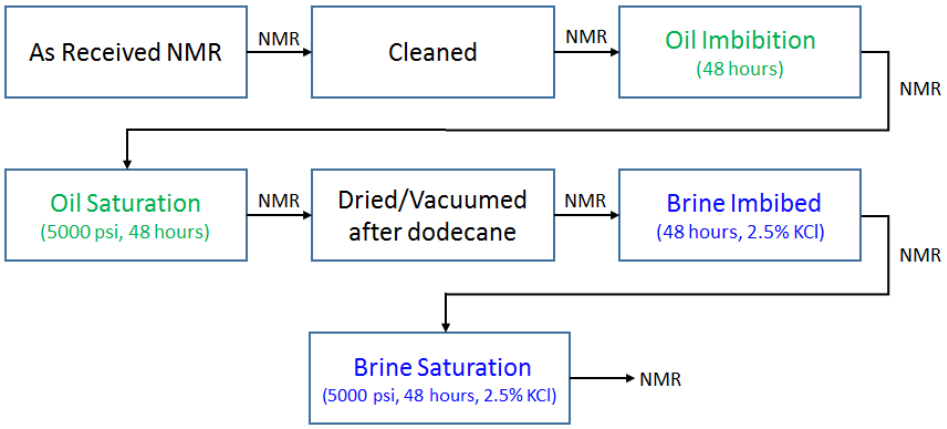

Figure 24— Experimental procedure designed for NMR data acquisition in Woodford Shale.

NMR Measurements at Elevated Pressures (TMS)

In the previous NMR experiments, samples were hydrostatically pressurized to 5000 psi, and removed from the pressure vessel to perform NMR measurements at atmospheric pressure. In rocks that are strongly non-wetting to dodecane, such as TMS, dodecane could be removed from the samples after the saturation pressure decreases to values lower than the average capillary pressure in a process known as "retraction" (Reeves and Celia, 1996). In order to test this hypothesis we acquired the NMR T_2 distribution (TE = 0.2 ms) of sample xxx35 under a dodecane pressure of 3500 psi and a confining pressure of 5000 psi. Based on the Washburn equation, it appears that dodecane can enter pore throats larger or equal to 4 nm at 3500 psi. The apparatus used to conduct the NMR measurements under pore and confining pressures is described in **Figure 25**. Prior to the NMR measurements, the sample was subjected to a methanol (20%) and toluene (80%) solvent extraction process at 130 °C and 1500 psi.

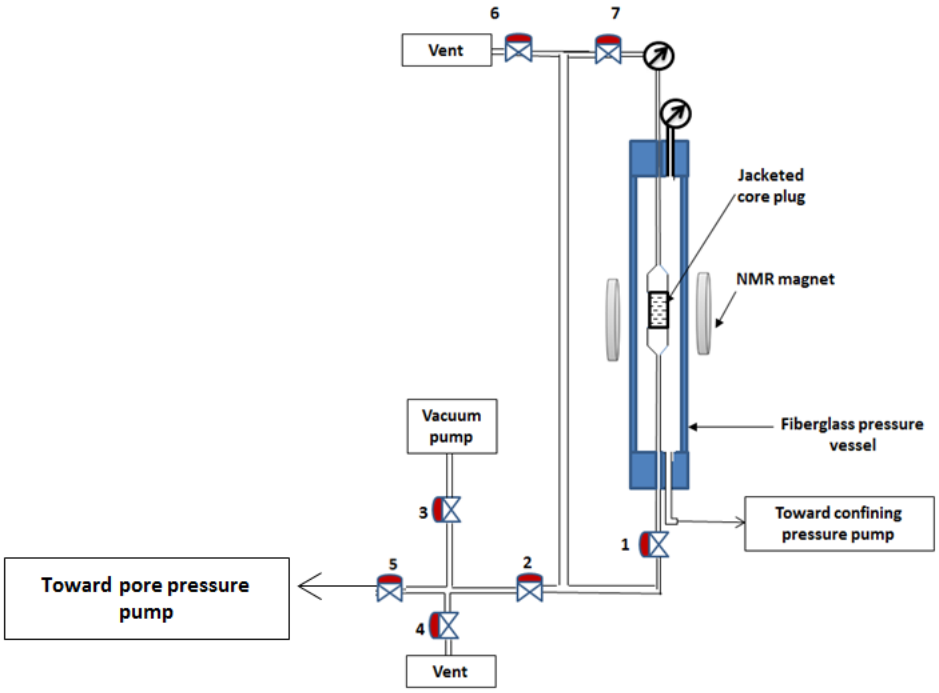

Figure 25 — Schematic of the experimental setup used to acquire NMR data under confining and pore pressures. Prior to saturation with dodecane, the confining pressure was raised to 5000 psi, and the sample was vacuumed for an hour by opening all valves except valve 4, 5 and 6. Fluorinert FC 770 was used as the confining pressure fluid. The sample was saturated by opening valve 5, closing valve 3 and applying a dodecane pressure of 3500 psi for 24 hours.

Chapter 5: Results and Discussion

Echo Spacing in Shales and Extrapolation to TE = 0

Kleinberg et al. (1993) reported on the enhanced diffusion relaxation with increasing echo spacing in large pores and the "dead time" phenomena where small pores relax before the acquisition of the first echo.

Using echo spacing of 114 μs and 600 μs, we measured the NMR T_2 response in Woodford shale and Berea sandstone. Results are compared in **Figure 26.** The top two figures show raw NMR signal obtained in Berea sandstone (left) and Woodford Shale (right). In Berea, measured porosity for both TE values is within 0.1 p.u and T_2 distributions are almost overlapping. Enhanced diffusion is observed in a slightly lower porosity and faster relaxation peak amplitude when TE = 600 μs. In Woodford shale, shorter echo spacing clearly identified presence of additional porosity, amounting to 3.7 p.u. At TE = 600 μs, nanopores relax before the first "Hahn's" echo is acquired and are unaccounted for due to the "dead time" phenomena. Field logging tools acquiring raw data using large TE values significantly underestimate porosity in shales.

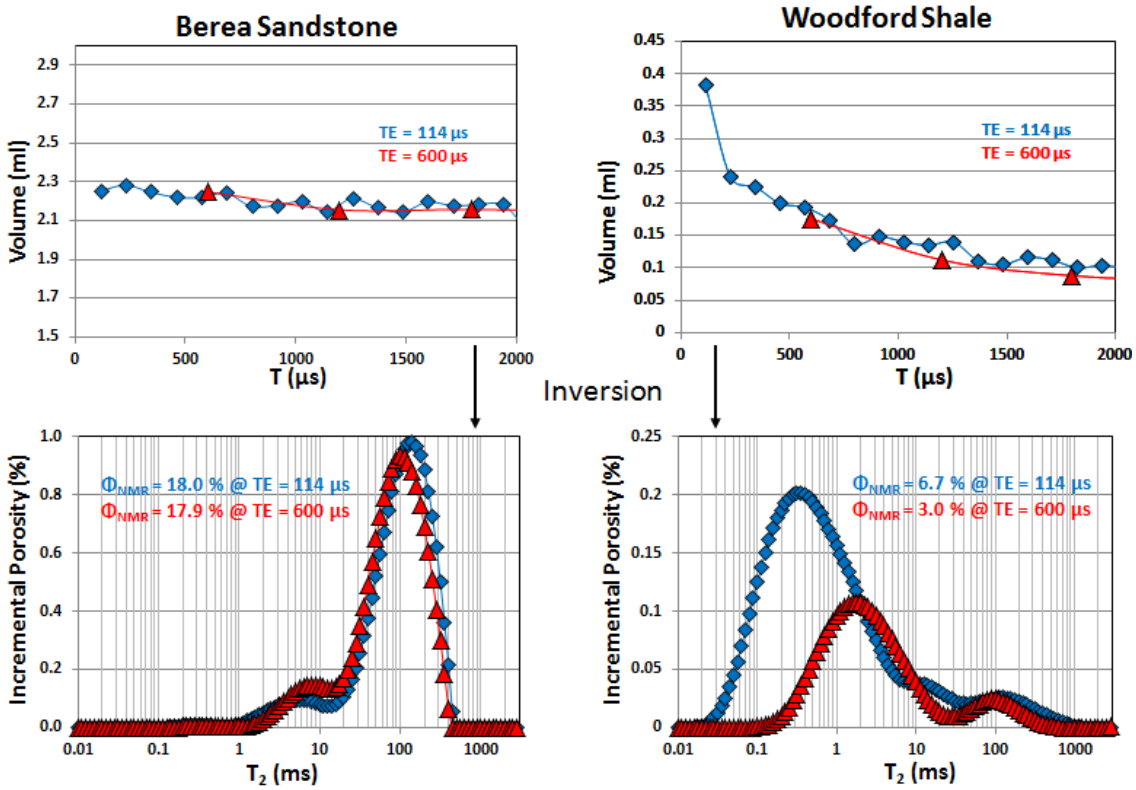

Figure 26— Top two figures show raw NMR signal obtained in Berea Sandstone (left) and Woodford Shale (right). Data is shown only for the first 2 ms to illustrate significance of echo spacing on measured signal. Porosities measured in Berea are within 0.1 p.u. and T_2 distributions are near overlapping. Shales show significant dependence of reported porosities on echo spacing.

In theory, porosity measured at zero relaxation time in the T_2 domain should provide total hydrogen count in the sample. However, due to ringing of the NMR probe and other electronic interferences, laboratory NMR measurements with GeoSpec2 are limited to 0.114 ms. MRIL and CMR-Plus logging tools are limited to 0.6 ms and 0.2 ms, respectively. Additionally, first echo in the field measurements is effected by 90 degree ringing and is neglected in processing (Freedman et al., 1997; Freedman et al., 1998). Service companies apply algorithms to extrapolate the spin echo envelope of the CPMG sequence acquired with logging tools to time zero, TE = 0 (Blumich et al., 2014; Schon,

2004; Dolinsek et al., 2006). Laboratory experiments conducted in this study do not rely on the extrapolation techniques.

As observed in Figure 26, extrapolation of raw data (top figure) to TE = 0 shows negligible change in porosity for a conventional rock, like Berea sandstone. In Woodford shale, extrapolation to zero time would result in significantly higher porosity. Notice that the first data point acquired at TE = 114 μs follows a different trend line compared to the trend at TE = 600 μs. Therefore, extrapolation practices should be conducted with caution in shale reservoirs.

NMR data was obtained at three different echo times in the TMS sample xxx86.7. Results are displayed in **Figure 27**. Porosity increases from 1.1 p.u. to 4.5 p.u. with decreasing TE values. Additionally, mean relaxation peak shifts from 0.8 ms to 0.3 ms. In conventional reservoirs, T_2 cutoff values are often applied to distinguish movable and residual fluids. Based on the results displayed in Figure 27, in shale reservoirs cutoff values are non-unique and are a strong function of echo spacing. This affects the interpretation of bound and movable fluids. Assuming a T2 cutoff of 0.8 ms, larger echo spacing overestimates movable fluid contents by 45.2% Therefore, E&P companies should carefully consider echo spacing when requesting laboratory NMR measurements. In order to tie results between laboratory and field measurements in shales, data should be acquired at the same TE values.

Results from the laboratory NMR measurements at two different echo times are cross-plotted in **Figure 28.** Porosity is consistently higher with shorter TE values. Additionally, two independent trends are observed, diverging at 1.5 p.u. on the x-axis. The presence of

obvious outliers shows that extrapolation of raw data to zero time is not unique and could cause significant errors in porosity estimation.

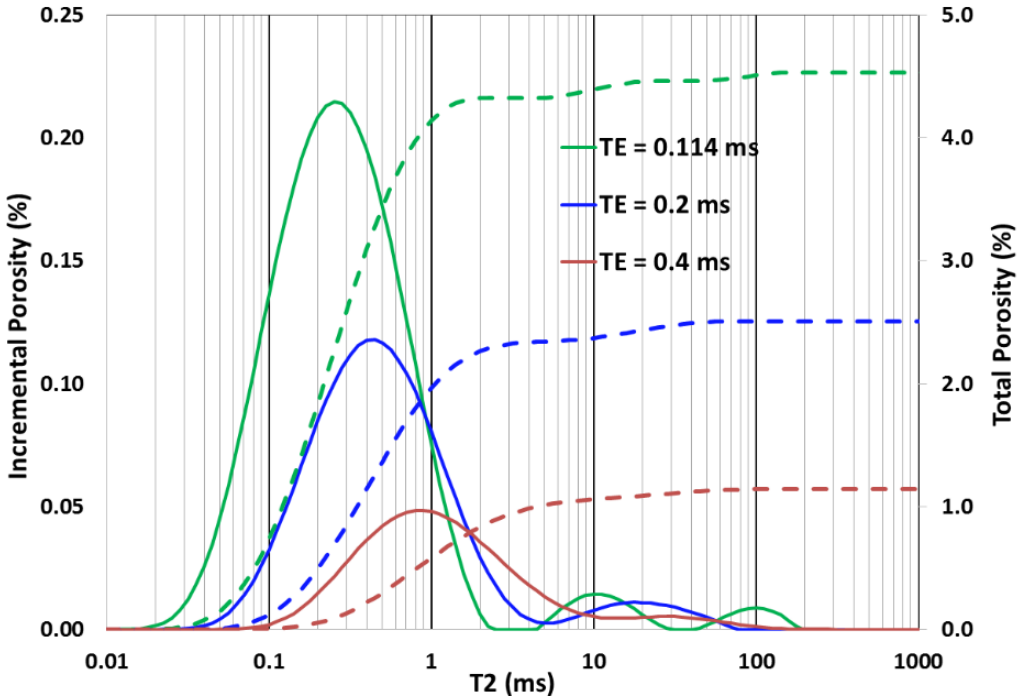

Figure 27 —T_2 relaxation response in the TMS sample xxx86.7 as a function of echo spacing. Mean relaxation peak shifts from 0.8 ms to 0.3 ms. Porosity ranges from 1.1 p.u. to 4.5 p.u as echo time is changed from 0.4 ms to 0.114 ms.

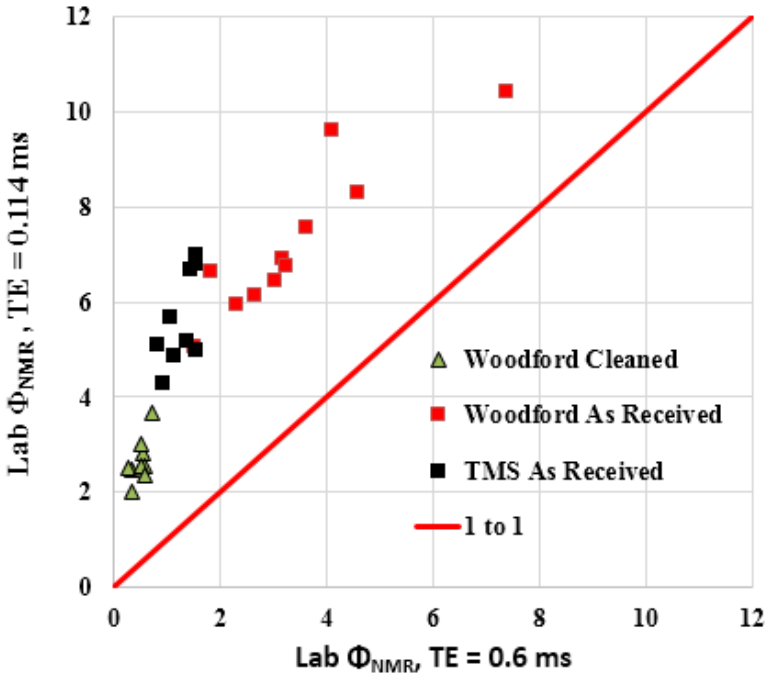

Figure 28 — Laboratory NMR porosities measured at TE = 0.6 ms and 0.114 ms. Results show consistently higher porosity reported with smaller TE.

T_2 Data Interpretation: Woodford Shale

Laboratory NMR spectra of the Woodford shale samples in the "as received", imbibed with oil and brine, as well as pressure saturated at 5000 psi are shown in **Figure 29 — Figure 32**. T_2 NMR spectra for the remaining Woodford samples can be found in "Appendix B".

The two field MRIL processing methods are overlaid with a laboratory "as received" data measured at TE = 0.114 ms in **Figure 29A** and TE = 0.6 ms in **Figure 29B**. The mean T_2 value of the "as received" core plug shifted to longer relaxation times with increasing TE values. The position of the dominant NMR amplitude in the field and laboratory data overlap around 1ms when the selected laboratory and field TE values are the same for both of the measurements (0.6 ms).

Results from dodecane imbibition and pressurized saturation at 5000 psi are shown in **Figure 30.** Regardless of the applied echo spacing, samples showed negligible change in fluid saturations. Observed relaxation times for the dodecane injected into samples range from 0.1 – 1000 ms. At TE = 0.114 ms, relaxation times below 1 ms represent nanoporosity. Macrofractures are apparent as T_2 values approach 1000 ms. At TE = 600 ms, nanopores remain undetected due to the "dead time" phenomena, while contribution from microporosity is present between 0.1 ms to 20 ms.

Samples were air-dried and vacuumed after the dodecane experiments. Results from the brine imbibition and pressure saturation with brine at 5000 psi on the dried samples are shown in **Figure 31.** Samples show a preferred affinity for water compared to dodecane as observed by significant change in porosity during brine saturation. At TE = 0.114 ms, the sample absorbed 2.2 p.u. of brine compared to 0.7 p.u. of dodecane. Water-wet pores reside at relaxation times between 0.1 ms and 10 ms.

Results from all of the laboratory NMR measurements for sample 3883 are shown in **Figure 32**. Following pressurized solvent extraction to remove residual fluids, measured porosities are consistently lower compared to "as received" porosity. Generally, sample cleaning with solvents is desired prior to porosity measurements to account for pores filled with viscous oils and bitumen. Woodford samples in this study are at the onset of oil generation window and have an average S2 = 53.7 mg/g and TOC = 7.7 wt% as observed in Table 6. We observed that sample cleaning restricted access to the initial pore network. Bitumen is soluble in organic solvents; however, its precipitants likely restricted access to the initial pore network.

In Figure 30 and Figure 31, it is apparent that T_2 relaxations of brine and dodecane residing in the Woodford samples overlap. Clearly, 1D T_2 measurements are not effective in distinguishing the types of fluids in the early maturity Woodford shale.

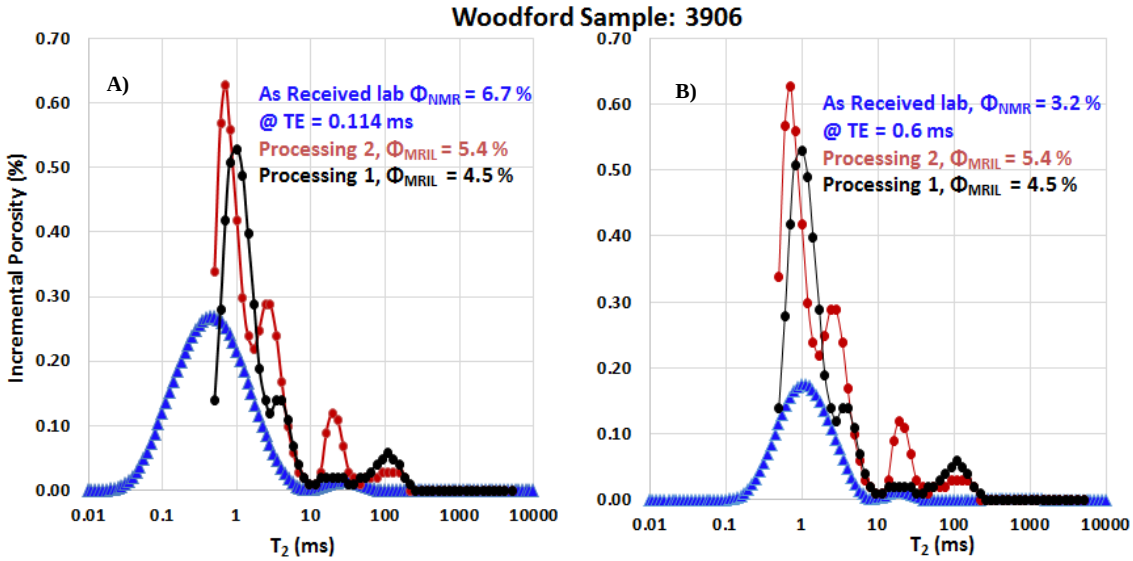

Figure 29— NMR T_2 distribution spectra for the two processing methods from the field and "as received" laboratory sample measured at A) TE = 0.114 ms on the left and B) TE = 0.6 ms on the right. The mean T_2 value of the "as received" core plug shifted to longer relaxation times with increasing TE values. The position of the dominant NMR amplitudes in the field and laboratory data overlap when their TE values are equivalent.

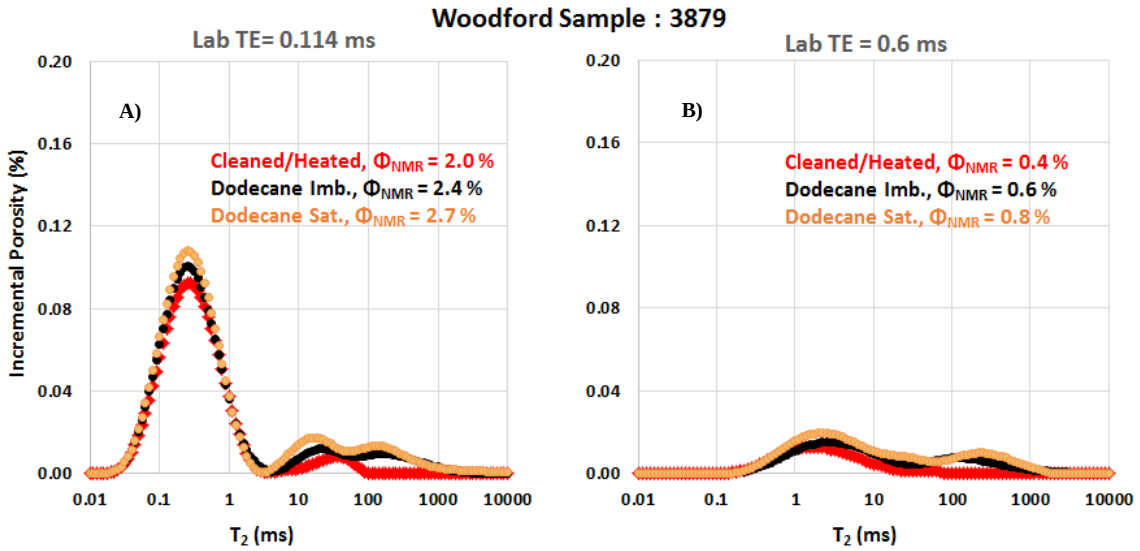

Figure 30 — Laboratory oil imbibed and pressure saturated NMR results A) at TE = 0.114 ms and B) at TE = 0.6ms measured on the same sample. Regardless of the applied echo spacing, samples showed negligible change in fluid saturations. Observed relaxation times for the dodecane injected into samples range from 0.1 – 1000 ms, capturing signal from nanopores to macrofractures, respectively.

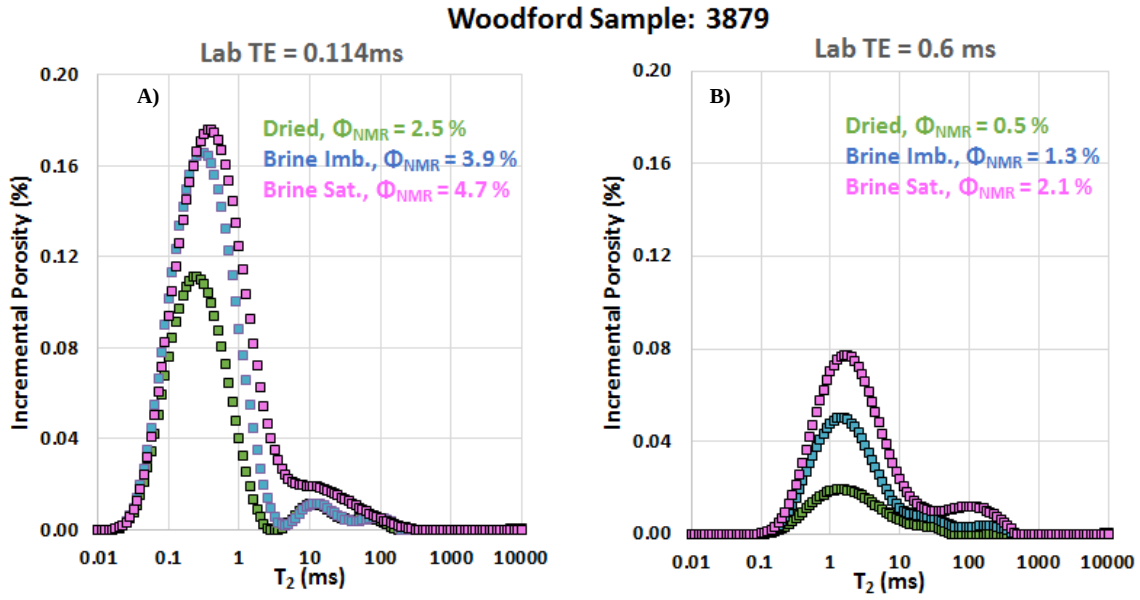

Figure 31 —Laboratory brine imbibed and pressure saturated NMR results A) at TE = 0.114 ms and B) at TE = 0.6ms measured on the same sample. Samples are preferentially water wet as observed by a significant change in porosity (porosity increased by 2.2 p.u. with brine compared to 0.7 p.u. with dodecane). Water-wet pores reside at relaxation times between 0.1 ms and 10 ms.

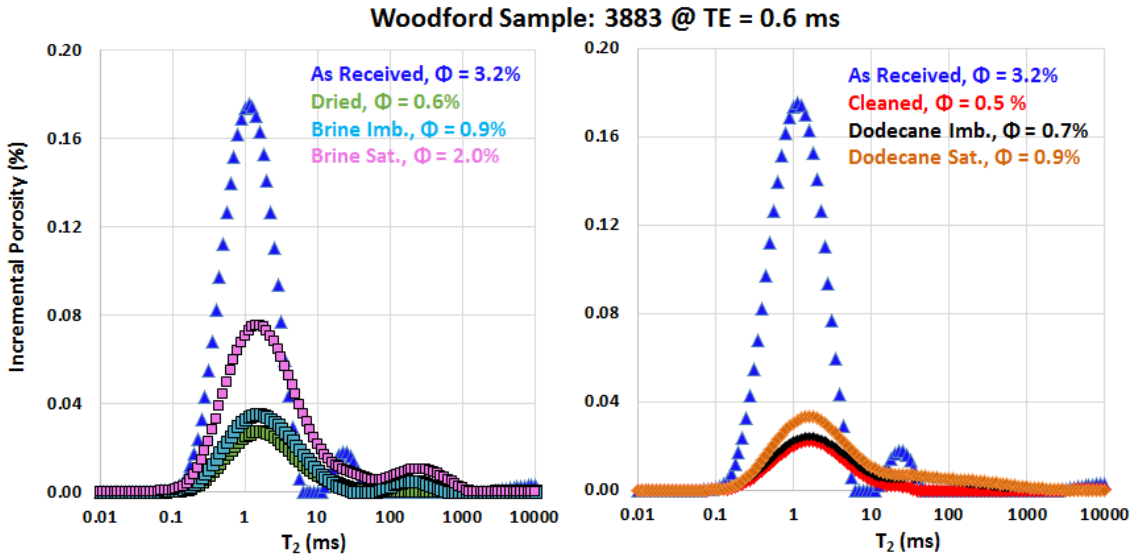

Figure 32 — Results from all of the laboratory NMR measurements shown for sample 3883. Following pressurized solvent extraction to remove residual fluids, measured porosities are consistently lower compared to "as received" porosity. Precipitants from mobilized bitumen likely restricted access to the initial pore network.

Interpretation of T_1-T_2 maps: Woodford Shale

Summary of the T_1-T_2 maps for six different samples in the "as received" state are displayed in **Figure 33.** Fluid saturations are unknown in the "as received" state, however all but two samples show T_1/T_2 signature at or above the 5:1 line (3951 and 3879). This suggests that hydrocarbons are likely dominating the NMR signal; however, results from dodecane imbibition and pressure saturation are examined below to investigate the hydrocarbon signature into these rocks.

Results of the T_1-T_2 maps after cleaning samples in three cycles (total duration of 5 hours) with a toluene and methanol mixture at 100 ^oC and at a pressure of 1500 psi are shown in **Figure 34**. Samples show T_1/T_2 ratio of 30 or above, representative of non-movable hydrocarbons that were unable to be removed/accessed with solvents. In the cleaned 3951 sample, two separate signals are apparent. Stronger amplitude represented by the irreducible brine, also observed in an "as received" state in

Figure 33. The second amplitude is the signal from non-movable hydrocarbons as observed in the other samples. It is important to note that non-movable hydrocarbons were not identified in the "as received" state in the T_1-T_2 maps.

Figure 35 shows summary of the T_1-T_2 difference maps for six different samples, generated by subtracting the brine imbibed data from the dried data. It is apparent that brine signal is residing at the T_1/T_2 ratio of 3 or below. Additionally, **Figure 36** shows difference maps for the same six samples where pressure saturated brine data was subtracted from the brine imbibed data. T_1/T_2 ratio for the brine that was forced into the rock at 5000 psi is also generally at a value of 3 or below.

Most of the samples did not intake significant amounts of dodecane, which is why **Figure 37** show results for only four samples. Samples imbibed with dodecane generally show a T_1/T_2 signature at or above 5:1 line. A significant portion of the signal is apparent above T_2 = 100 ms, most likely from the dodecane residing in the microfractures. Fluids in the pore matrix, below 10 ms, also show a T_1/T_2 ratio above 5.

Dodecane was forced into the matrix by applying hydrostatic pressure of 5000 psi. Small, non-wetting pores are accessed through pressurized saturation, on the order of 2.8 nm (Washburn's equation) when pressurized with dodecane at 5000 psi. In **Figure 38**, injected dodecane has T_1/T_2 ratios of 10 or above. It seems that hydrocarbons forced into the smaller water wet pores experience a larger T_1/T_2 contrast. These results are consistent with Nicot et al. (2016) and Anand et al. (2015) who reported that high T_1/T_2 ratios are not necessarily due to the presence of viscous hydrocarbons or bitumen but rather due to the fluid confinement in nanopores. Low viscosity hydrocarbons confined to nanometer size pores experience increasing correlation times, τ_c, shown in Figure 1, or decreasing

rotational mobility. This results in the increasing T_1/T_2 ratio contrast. Additionally, non-movable hydrocarbons, which remained in the Woodford samples following pressurized cleaning with solvents, showed $T_1/T_2 \geq 30$. Therefore, in nanometer size pores, T_1-T_2 signatures of low viscosity hydrocarbons and viscous hydrocarbons are likely to overlap. Samples also exhibit additional signal in the lower right corner of Figure 38. This is an artifact of subtraction algorithms and does not represent real data.

Figure 39 shows summary T_1-T_2 data summary for one of the samples in various states of saturation: "as received", cleaned, dodecane imbibed and pressure saturated, dried, imbibed and pressure saturated with brine. Main signal is above the 5:1 T_1/T_2 line. Based on the spontaneous imbibition and pressure saturation experiments with dodecane shown in the Figure 37 and Figure 38, the NMR signal is likely dominated by hydrocarbons. Non-movable hydrocarbons are identified in the "cleaned" sample state, where amplitude is generated at a T_1/T_2 ratio of 35. Those hydrocarbons were not mobilized or dissolved during pressurized solvent extraction with an 80/20 toluene/methanol mixture at 100 ^{o}C and pressure of 1500 psi. In the dodecane saturated core plug, new signal is noticeable at the 5:1 T_1/T_2 line. After air-drying and vacuuming the sample, some of the dodecane remained in the pores, represented in the light blue shade. After sample saturation with brine at 5000 psi, T_1/T_2 ratio decreased to a value of 3.

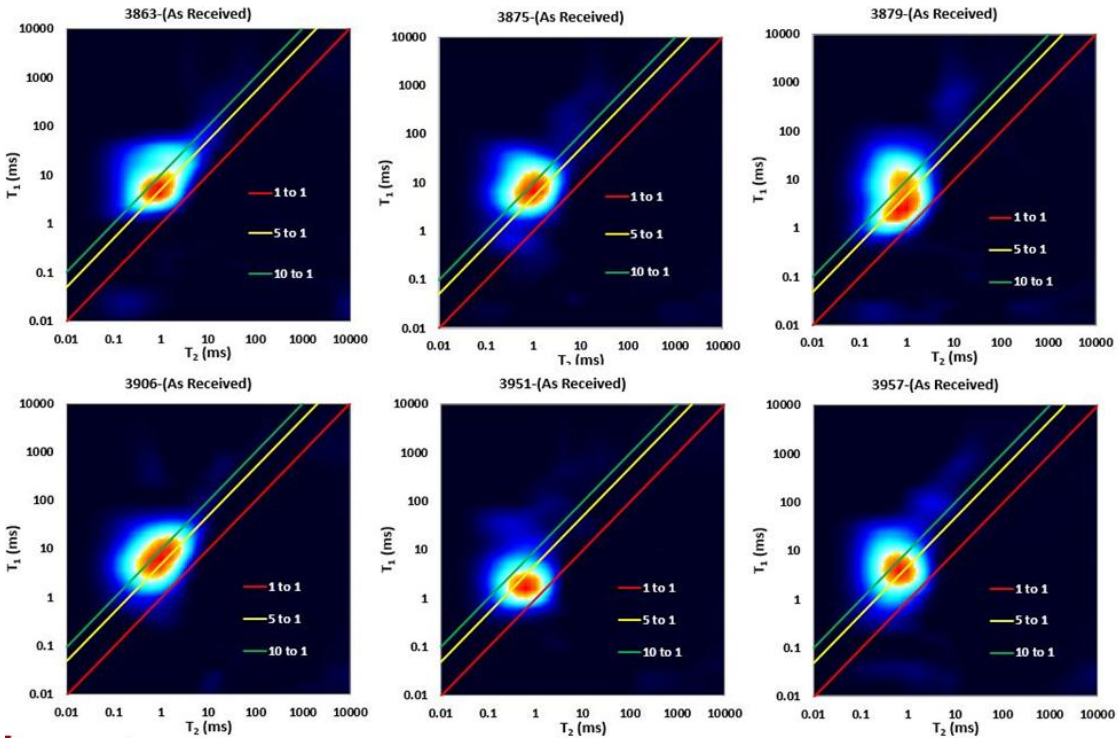

Figure 33 —T_1-T_2 maps for six different samples in the "as received" state. Fluid saturations are unknown in the "as received" state, however all but two samples show T_1/T_2 signature at or above the 5:1 line (3951 and 3879), suggesting that hydrocarbons are likely dominating the NMR signal.

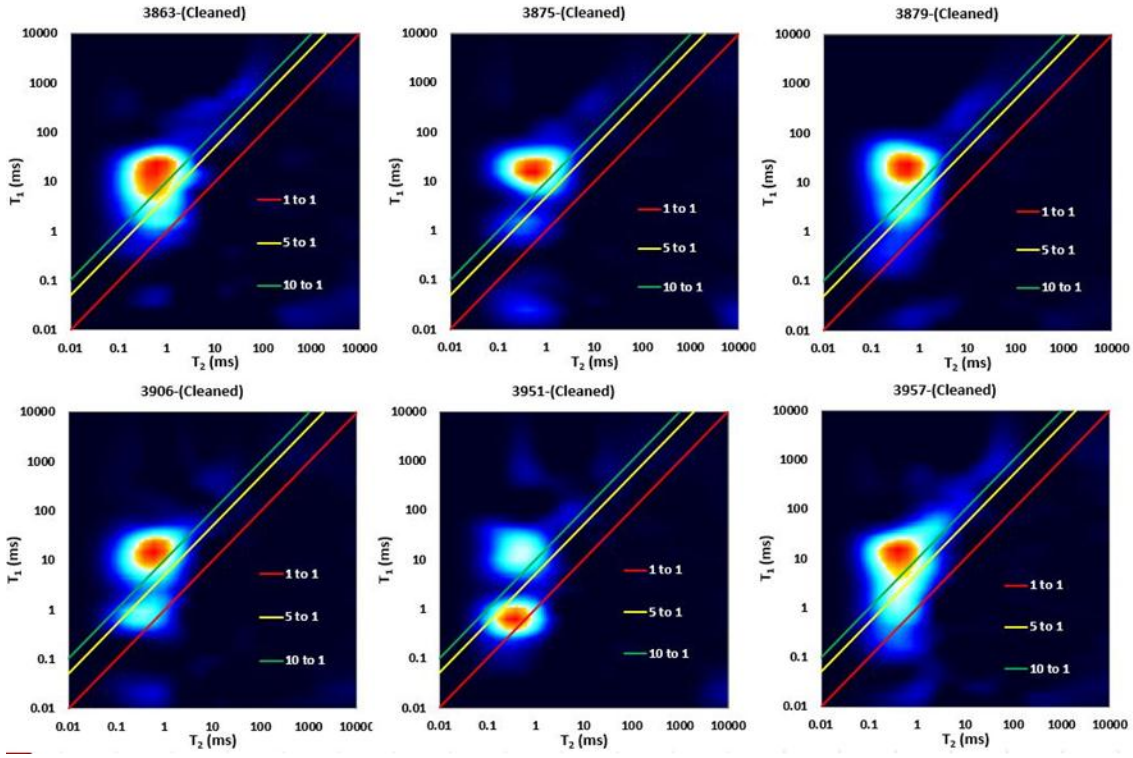

Figure 34 —T_1-T_2 maps for six different samples following the sample cleaning. Samples show T_1/T_2 ratio of 30 or above, representative of non-movable hydrocarbons that were unable to be removed/accessed with solvents. Two amplitudes are observed in samples 3906 and 3951: second peak (closer to 1:1 line) is representative of the irreducible brine, in addition to the signal from non-movable hydrocarbons.

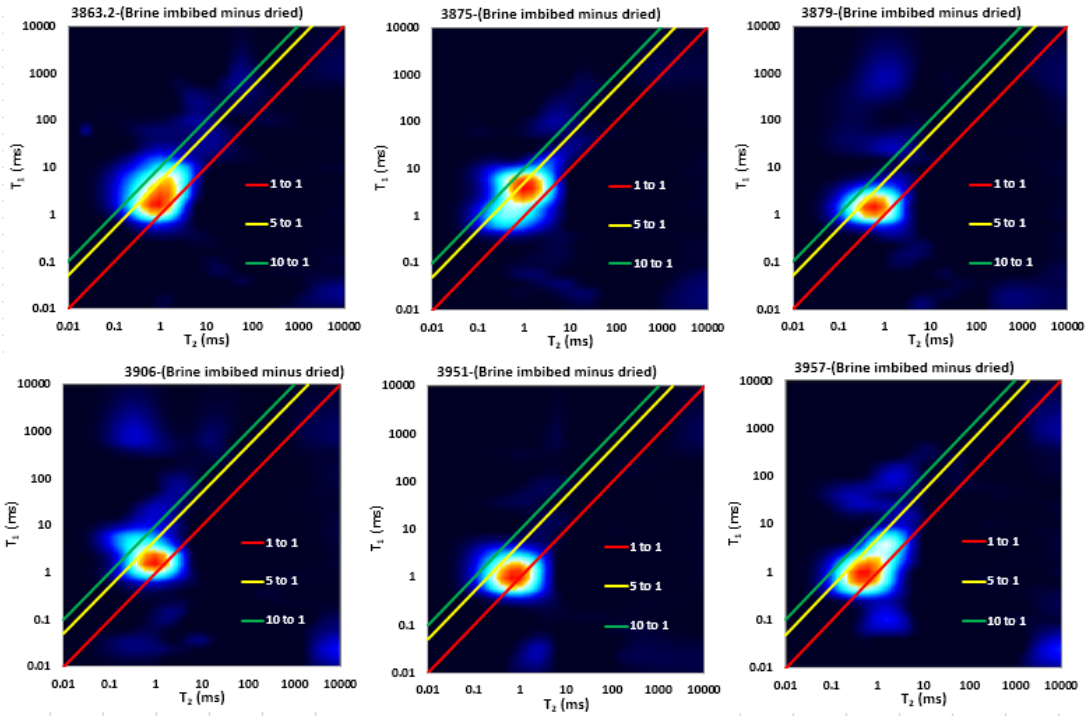

Figure 35 — T_1-T_2 difference maps for six different samples: brine imbibed – dried. Imbibed brine is residing at the T_1/T_2 ratio of 3 or below.

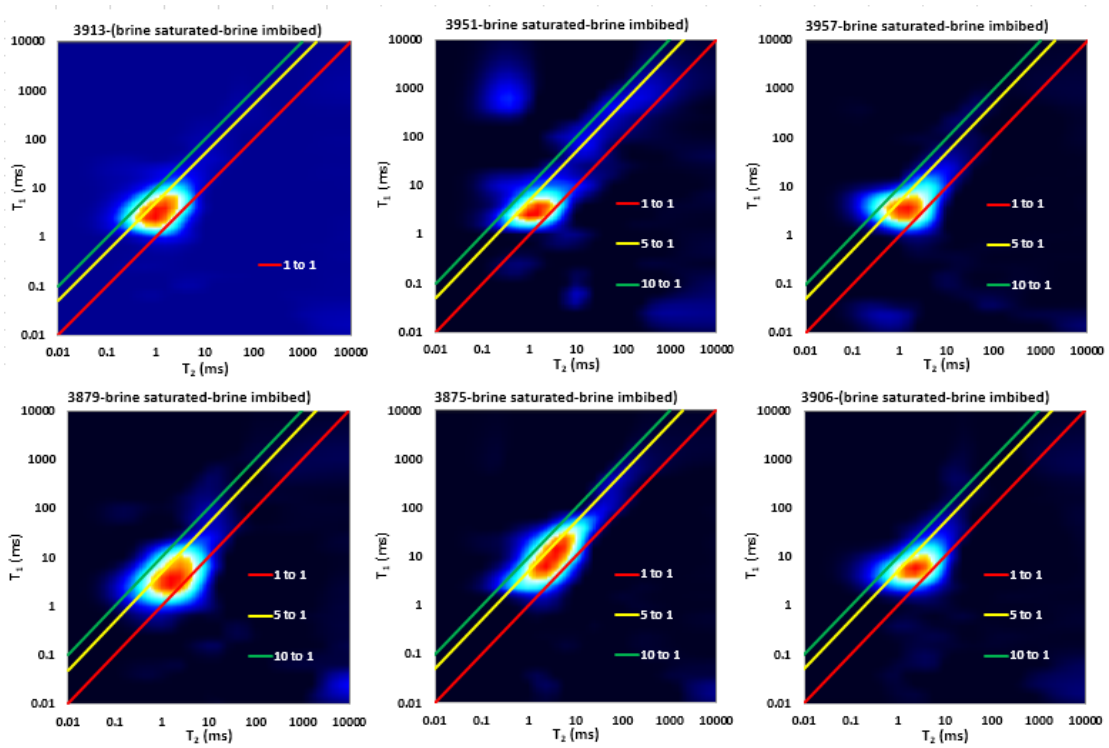

Figure 36 – T_1-T_2 difference maps for six different samples: brine pressure saturated at 5000 psi - brine imbibed. T_1/T_2 ratio for the brine forced into the rock at 5000 psi is below or at a value of 3.

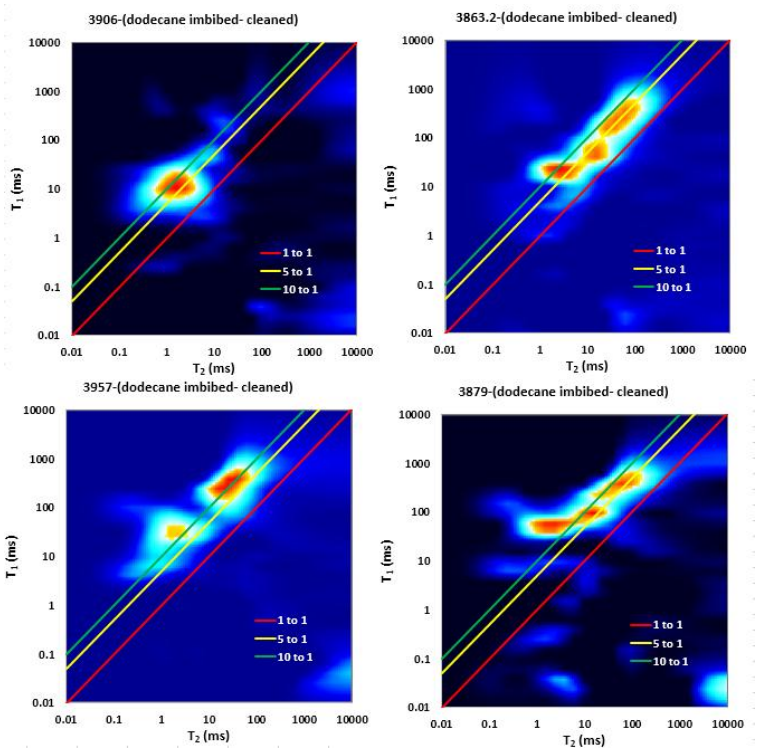

Figure 37 — T_1-T_2 difference maps for four different samples: dodecane imbibed – cleaned. Samples generally show a T_1/T_2 signature at or above 5:1 line. A significant portion of the signal is apparent above T_2 = 100 ms, most likely from the dodecane residing in the microfractures. Fluids in the pore matrix, below 10 ms, also show a T_1/T_2 ratio above 5.

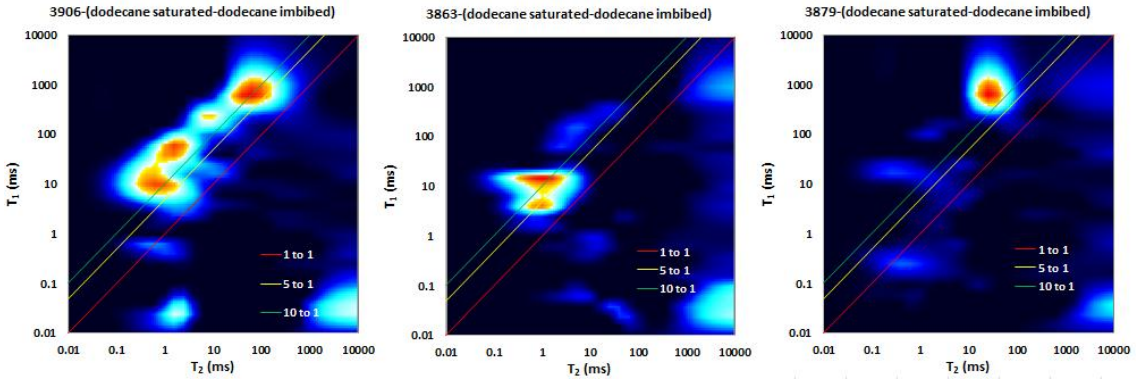

Figure 38 — T_1-T_2 difference maps for three different samples: dodecane pressure saturated - dodecane imbibed. Injected dodecane has T_1/T_2 ratios of 10 or above. It seems that hydrocarbons forced into the smaller water wet pores experience a larger T_1/T_2 contrast due to decreasing mobility.

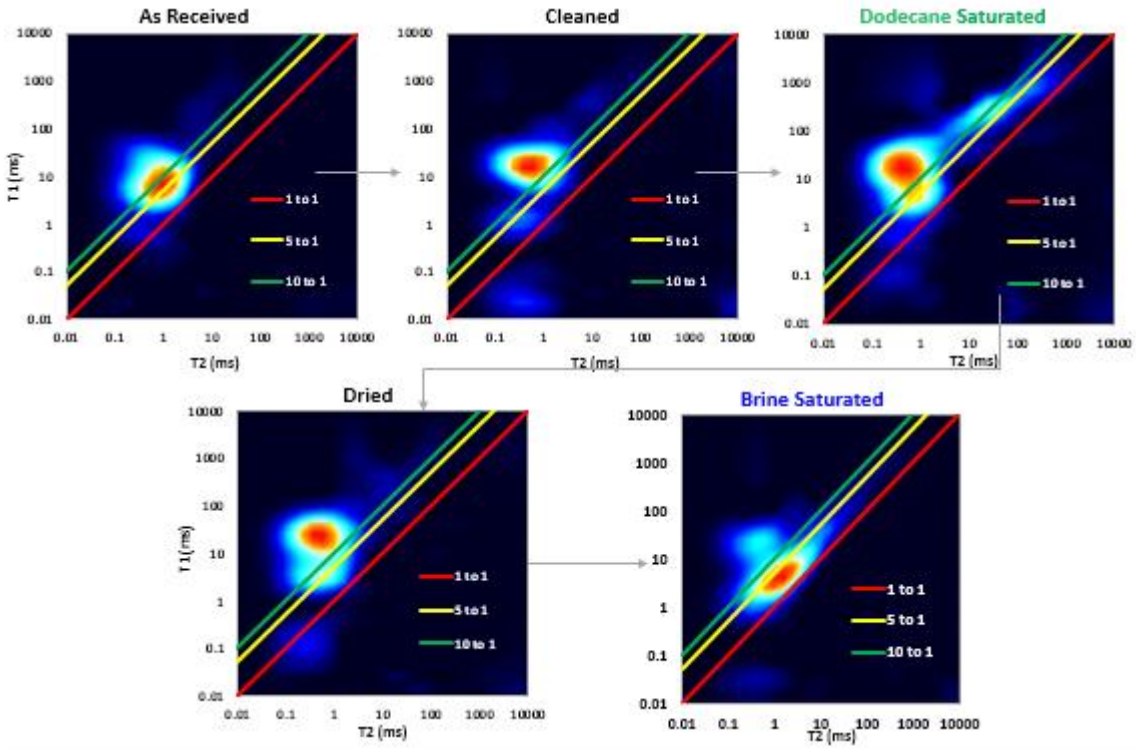

Figure 39 — T_1-T_2 NMR signature for sample 3875 measured in various saturation states. In the as received state, hydrocarbons are dominating the NMR signal, with T_1/T_2 signature above the 5:1 line. After sample cleaning, non-movable hydrocarbons exhibit T_1/T_2 ratios above the 30:1. Sample saturation with dodecane showed T1/T2 ratio above the 5:1 line, showing the effects of decreasing rotational mobility in the nanopores of shales. By saturating the sample with brine, T_1/T_2 ratio decreased to a value of 3.

T_2 Data Interpretation: Tuscaloosa Marine Shale

Examples of laboratory T_2 NMR spectra of the TMS samples imbibed with brine are shown in **Figure 40A** and pressure saturated with dodecane in **Figure 40B.** In addition, porosity from the field CMR-Plus logging tool is overlayed on the laboratory data. **Table 7** shows results for 11 samples from the laboratory NMR measurements in various imbibition/saturation stages. T_2 NMR spectra for the remaining TMS samples can be found in "Appendix A".

"As received" laboratory NMR porosity is less than field CMR log porosity by an average of 4.2 p.u., which suggests that a significant portion of reservoir fluids escaped from the samples between core acquisition and laboratory measurements.

In Figure 40A, due to the fractures induced during brine imbibition, measured brine imbibed porosity (8.9%) is significantly larger than the field CMR-Plus porosities (7% and 5.7%). Contributions from fractures are captured at relaxation times above 10 ms. In order to mitigate the contribution from the induced fractures, the NMR response above 10 ms will be excluded in subsequent interpretations, as this signal is not a part of the matrix. Average brine imbibed porosity after applying the 10 ms cutoff is 7.1 p.u. Samples spontaneously imbibed large amounts of brine as the difference between the brine imbibed and "as received" porosity is 4.2. p.u. In the "as received state", fluids remaining in the samples are indicative of minimal irreducible water (S_{wir}). Therefore, 2.9 p.u., or 40.8% of the total porosity, is filled with irreducible water.

In Figure 40B, the overlapping T_2 distributions of the "as received" and dodecane imbibed samples suggest that dodecane was not imbibed. Furthermore, samples did not intake dodecane even after applying 5000 psi of hydrostatic pressure. Combined with the results from the spontaneous brine imbibition experiments (imbibed 4.2 p.u. of brine), TMS rock matrix is strongly water wet.

Results from the pressurized NMR experiment are shown in **Figure 41**. Following sample cleaning, 2.3 p.u. are occupied by the residual brine as measured in the "Cleaned & Dried" sample state by NMR. Dodecane saturation increased by 0.7 p.u. after applying 3500 psi of pore pressure and remained constant after the confining and pore pressures were released. Considering an error in the machine measurement of 0.5 p.u., change in

dodecane saturation is minimal to negligible. Combined with the results from the brine/dodecane imbibition and saturation experiments, due to the strong affinity to water, residual brine remaining in the TMS samples causes capillary blockage and prohibits hydrocarbon accessibility to the pore network.

Average laboratory brine imbibed NMR porosity with a 10 ms cutoff is 7.1 ± 0.9%, compared to average crushed helium porosity (Table 5) of 5.5 ± 0.9%. Prior to the crushed helium porosity measurement, samples are heated to 100 °C to remove free water. Residual water in the samples is the remaining "bound water", not removed from the samples at the temperature of 100 °C due to the surface forces and capillary pressure. NMR is measuring bound water as porosity, while crushed helium experiments account for bound water as part of the matrix. This explains the observed higher average porosity reported with NMR compared to crushed helium measurements.

Crossplots of laboratory measured NMR porosity and field CMR porosities are shown in **Figure 42**. Core data was depth-shifted prior to core and log data comparisons. Results indicate that reported porosities are within 2 p.u. of each other.

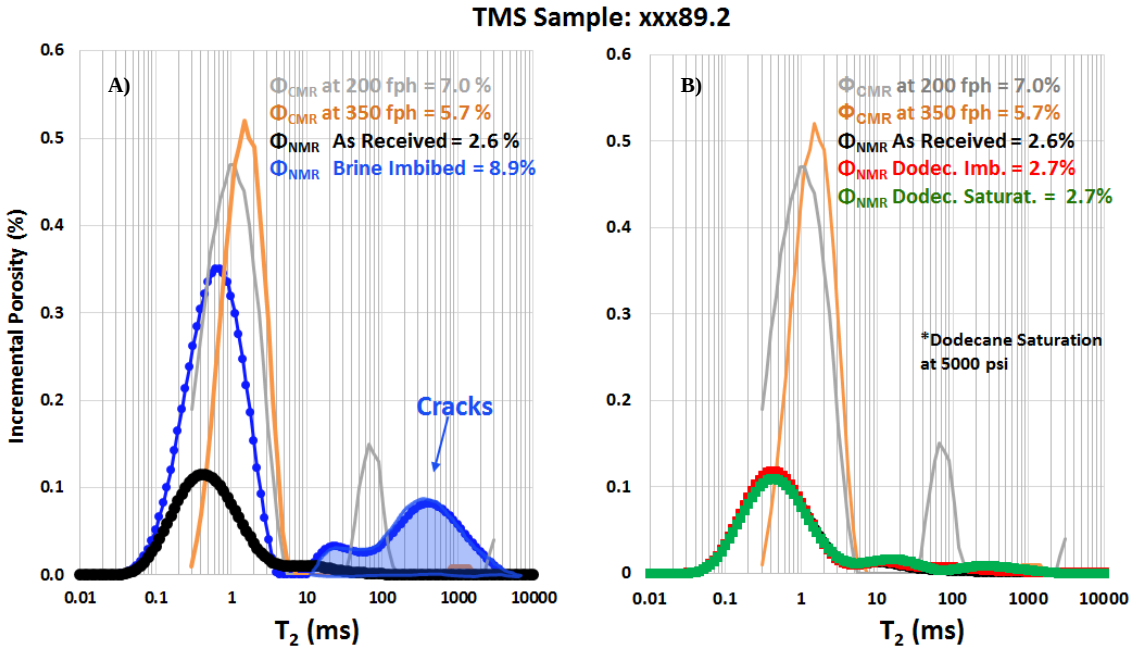

Figure 40—Representative laboratory NMR signatures of the 12 TMS samples after imbibing A) brine and B) dodecane. "As received" samples are on average 3 p.u. lower compared to porosity recorded with the CMR-Plus tool in the field. Brine imbibition generated fractures, which are captured above 10ms. Samples did not intake dodecane after spontaneous imbibition or pressurizing to 5000 psi.

Table 7—Summary of the laboratory NMR measurements in various samples of Tuscaloosa Marine Shale undergone imbibition/saturation with dodecane and brine.

Sample	xxx 86.7	xxx 89.2	xxx 91	xxx 34.5	xxx 35	xxx 40.0	xxx 75.5	xxx 80.0	xxx 11.4	xxx 12.2	xxx 14.8
As received NMR Φ (%)	2.5	2.6	2.7	3.0	3.3	2.9	3.5	3.9	2.5	3.0	1.9
Brine imbibed NMR Φ (%)	7.5	8.9	11.1	8.2	6.8	10.9	9.7	9.8	x	12.6	7.2
Brine imbibed NMR Φ with cutoff at 10 ms (%)	6.0	6.8	7.8	7.0	6.2	7.7	8.1	8.3	x	7.2	5.5
Dodecane imbibed NMR Φ (%)	2.6	2.8	2.9	3.1	3.3	2.3	3.2	3.3	x	x	x
Dodecane saturated NMR Φ (%)	2.6	2.7	2.9	2.9	3.2	1.8	3.1	3.3	2.4	2.9	1.8

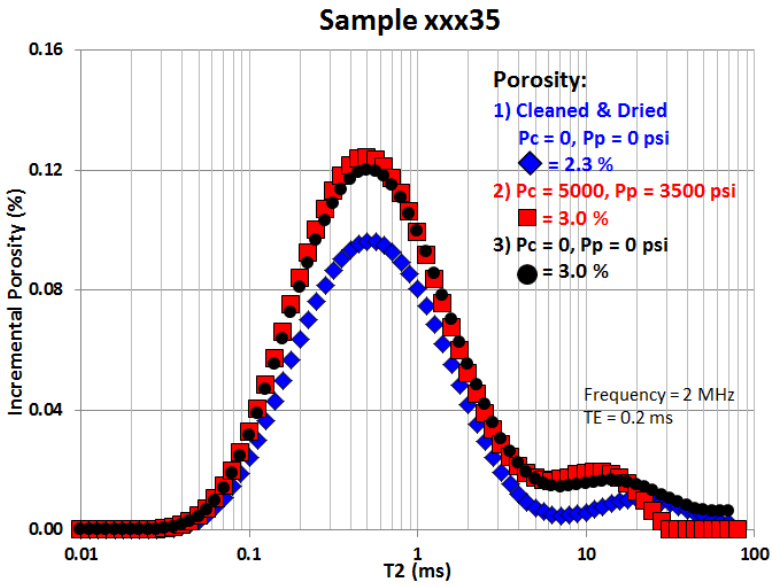

Figure 41—Incremental porosity from NMR measurement obtained at different pore pressures. Dodecane was used to generate pore pressure. Residual brine remaining in the TMS samples (2.3 p.u. in the "Cleaned & Dried" state) causes capillary blockage and prohibits hydrocarbon accessibility to the pore network.

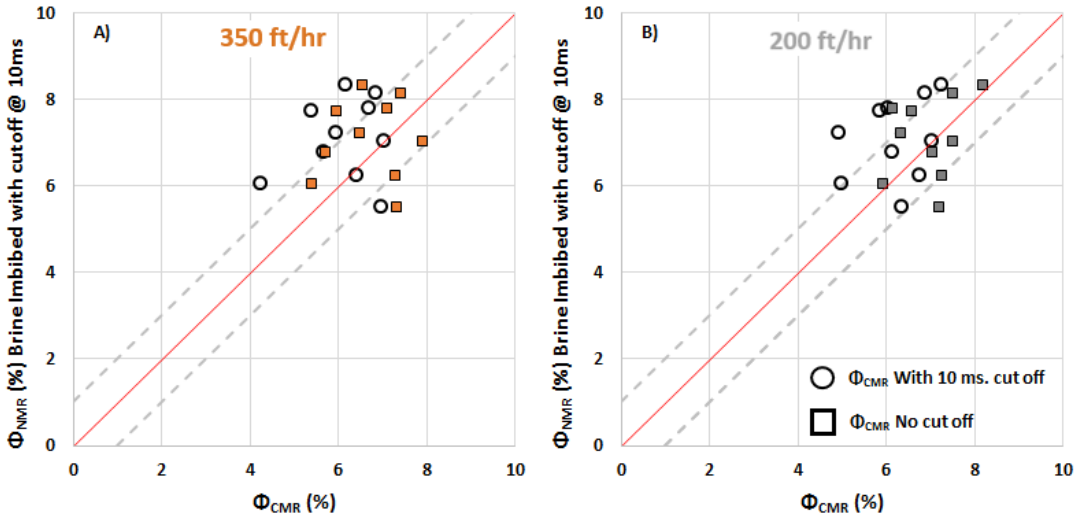

Figure 42— Laboratory NMR porosity compared to field CMR logs at 350 fph and 200 fph. Since fractures were induced in the core plugs after brine imbibition, contribution from the fractured porosity is removed by neglecting signal beyond 10ms. Results indicate that reported porosities are within 2 p.u.

Interpretation of T_1-T_2 maps: Tuscaloosa Marine Shale

Results from the T_1-T_2 maps measured on the TMS samples at TE = 0.114 ms are displayed in **Figure 43**. Residual fluid in the "as received" samples is unknown; however, the average T_1-T_2 ratio is 3 (Figure 43 A, B, C). Following imbibition by brine, porosity increased by an average of 3 p.u, while T_1-T_2 ratios remained around 3 (Figure 43 D, E, F). This indicates that most of the residual fluid in the core plugs is also brine. Ozen and Sigal (2013) measured the average T_1/T_2 = 2.2 on powdered Barnett samples imbibed with brine, which is slightly lower compared to the TMS brine imbibed ratios.

NMR experiments on the "as received" and "cleaned and dried" plugs suggest that TMS matrix cannot store hydrocarbons due to strong non-wetting behavior to hydrocarbons and capillary blockage by brine. Hydrocarbon production is likely coming from sources other than matrix porosity.

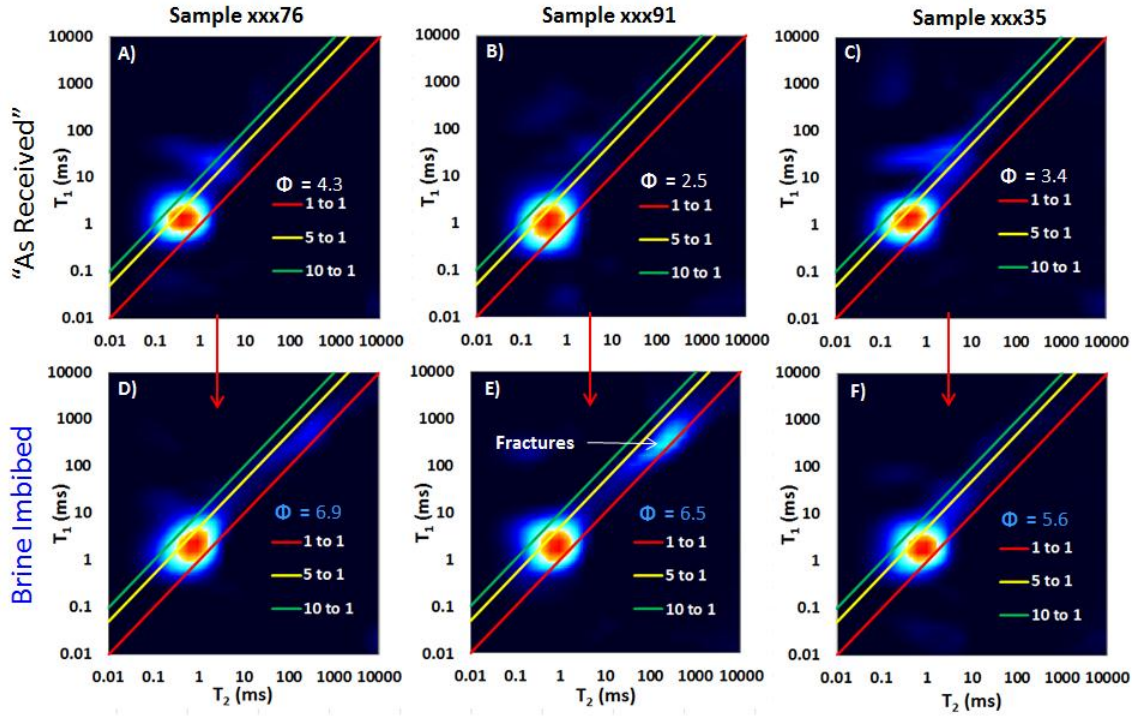

Figure 43—T_1-T_2 maps showing relaxation in "as received" samples (A, B, C) and brine imbibed samples (D, E, F) at TE = 0.114 ms. Following imbibition with brine, porosity increased by an average of 3 p.u, while T_1-T_2 ratios remained around 3. This indicates that most of the residual fluid in the core plugs is also brine. Additional signal is observed above 100 ms in brine imbibed sample xxx91, which is a contribution from the fractures induced during brine imbibition. T_1-T_2 porosities exclude fracture contribution (above 10 ms) from the total porosity.

TMS T_2 Spectrum: Sensor Alignment with Micro-Fractures

Additional NMR signal above 10 ms was observed with a slower logging run as shown in **Figure 44A.** In conventional water-wet reservoirs, longer relaxation typically corresponds to non-wetting hydrocarbons relaxing as a bulk fluid (Ostroff et al., 1999). Possibilities for additional signal at longer T2 times are: 1) fluids with longer relaxation times are underpolarized in the faster logging run; 2) CMR-Plus tool has a narrowly focused sensor, as shown in Figure 4. If slower logging run is oriented with the fluid filled vertical fractures, longer relaxation times become more apparent.

The possibility of fluid underpolarization was investigated. Field and laboratory measurements in Figure 40 were conducted with the same TE = 0.2 ms. Field data was acquired with 5000 echoes compared to laboratory range of 1250-5000 echoes. Laboratory wait times ranged from 0.5 sec to 1.5 sec and, as observed in Figure 40, were sufficient to polarize the fluid in the induced fractures under no confining pressure. This means that proton polarization with the logging tool should have been equal to or greater than 1.5 sec.

According to McKeon et al. (1999), when the tool collects data via overlapping PAPs, the effective polarization time is approximately the wait time of the applied pulse sequence. For data gathered through sequential PAPs, the effective polarization time is the time needed to travel 18 inches (average prepolarization for a 6-in antenna) (McKeon et al., 1999).

Tuscaloosa Marine Shale was logged in CMR-B mode collecting data in sequential PAPs. At 350 fph, effective polarization time is 15.4 sec. This was sufficient time to achieve complete proton polarization. Therefore, fluids were effectively polarized at the logging speed of 350 fph.

Additionally, a representative example of the resistivity image (NGI image log) over 15 ft. in the TMS is captured in **Figure 44B.** The image has been processed by a service company to highlight fractures (brighter colors, resistive) within the formation. Intervals with the abundant vertical fractures correlate with the intervals where the additional NMR signal is observed. Therefore, the presence of the additional signal is likely due to the orientation of the NMR sensor with the apertures in Figure 44B. Observed fractures could be filled with (1) connate water, (2) drilling fluids, (3) minerals, or (4) hydrocarbons:

1) Formation was drilled overbalanced with an oil based mud. In overbalanced drilling the borehole fluid pressure exceeds the formation pressure which can lean to fluid invasion. Based on the laboratory pressurization experiments with dodecane, the nanopores in the TMS matrix are not accessible to non-wetting hydrocarbons even at pore pressures of 5000 psi. However, open fractures would have been flushed with oil based mud, replacing the generally conductive connate water. This eliminates the possibility of connate water residing in the open fractures.

2) Resistive properties of the mud are as following: mud Rm = 500 ohm-m at 68 °F, Rmf = 375 ohm-m at 68 °F; where Rm is resistivity of the mud and Rmf is the resistivity of the mud filtrate. Mud resistivity at bottomhole temperature of 225 °F was 161 ohm-m. Average resistivity of TMS is 7.4 ohm-m with a range from 2.6-14.9 ohm-m. Therefore, in the presence of open fractures, fluid invasion by oil based mud would possibly explain the observed high resistivity response.

3) At the same time, azimuthal resolution of the image log is limited to 3.5mm, therefore the aperture of the observed high resistivity fractures would have to be equal to or greater than 3.5mm. A fluid filled fracture with an aperture of 3.5mm would generate an NMR response of unconfined bulk fluid with relaxation time (T_2) on the order of seconds, which were not observed on a CMR-Plus log. Intervals where additional NMR signal correlates with the vertical fractures show T_2 relaxation times at or below 350 ms, which is below the relaxation time of bulk fluids. This means that the 3.5mm fractures are most likely filled through mineralization by deposition of resistive minerals.

4) The T_2 response, generated by the CMR-Plus logging tool, with relaxation times of 10-350 ms is likely coming from microfractures filled with hydrocarbons. Microfracture

dimensions are below the resolution of the NGI image log, however, can be sensed by NMR when filled with fluids.

Additionally, notice the degree of vertical variability within the formation. Brighter colors are representative of the resistive intervals and could explain the elevated resistivity readings in the TMS which were observed by other authors (Lu et al., 2015; Allen et al., 2014).

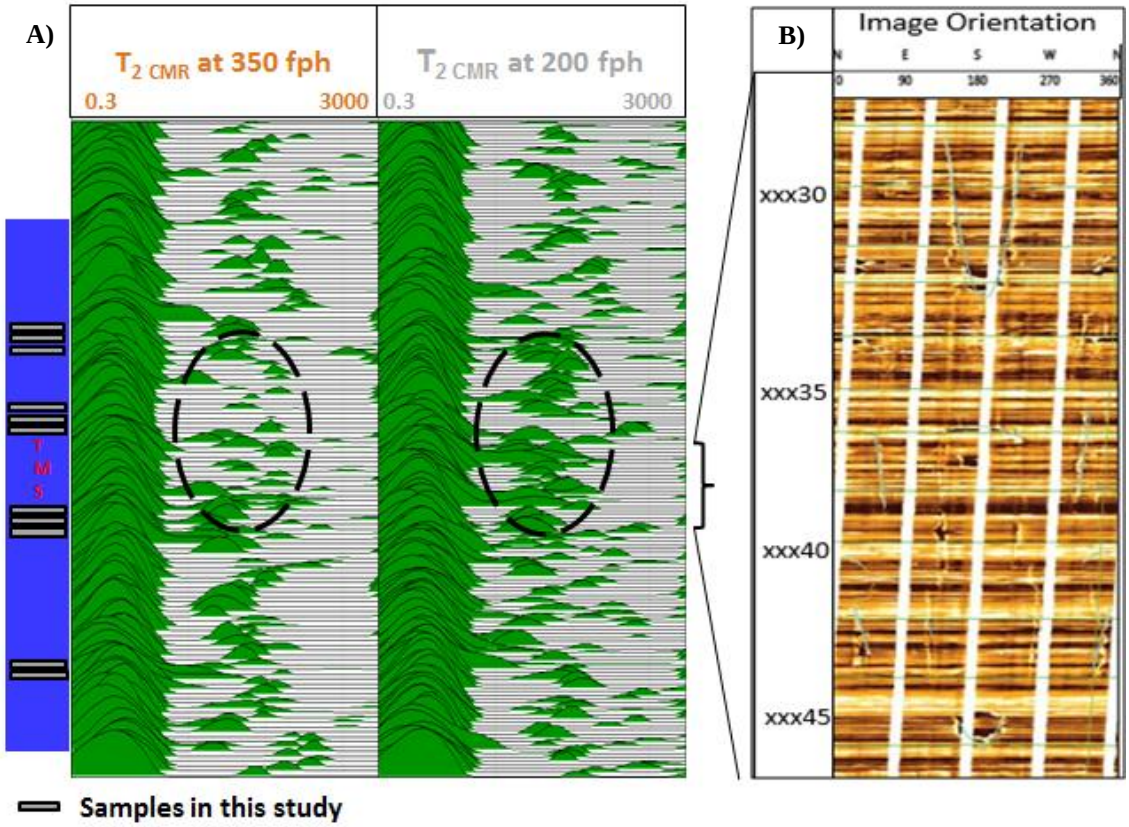

Figure 44—A) Additional signal is apparent above relaxation times of 10ms in the slower logging run. B) NGI log (resistivity based image log) highlighting vertical fractures and high occurrence of laminations within the formation.

Chapter 6: Conclusions

Summary

Low field laboratory NMR measurements were conducted on the Tuscaloosa Marine Shale (prime oil generation window) and Woodford Shale (onset of hydrocarbon generation). 1D T_2 measurements at various echo spacings (TEs) and T_1-T_2 maps were obtained to address fluid typing and storage capacity in shales. NMR signals were gathered in the following sample states: as received, following sample cleaning, brine imbibed and saturated, imbibed and pressure saturated with dodecane. Results were compared and integrated with to the field data from CMR-Plus, MRIL and NGI image logs.

Echo Spacing Effect on Shales

T_2 measurements in shales show that echo spacing has a significant impact on the measured storage capacity. Minimum TE resolution with our laboratory instrument is 114 μs, compared to the field MRIL-Prime tool TE = 600 μs. This results in an underestimation of over 70% of the storage capacity in shales. Service companies correct for echo spacing by extrapolating TE = 0; however, we showed that extrapolation practices should be conducted with caution or avoided in shale reservoirs.

Additionally, echo spacing effects not only the amplitude of the measured signal but also shifts the T_2 distribution to faster relation times. In conventional reservoirs, T_2 cutoffs are often applied to distinguish movable and residual fluids. In shales, cutoffs are non-unique and are a strong function of echo spacing. In order to tie results between laboratory and field measurements data should be acquired at the same TE values.

Woodford Shale Results

Woodford shale was cored from the shallow section of the Arkoma basin at the onset of oil generation window. Samples showed more affinity to brine compared to dodecane. Water-wet pores are residing between the T_2 relaxation times of 0.1 ms and 10 ms. 1D T_2 measurements were not effective in distinguishing types of fluids in the early maturity window. T_1-T_2 measurements on brine imbibed and pressure saturated samples at 5000 psi generally showed T_1/T_2 ratios below 3. Results from dodecane imbibition showed T_1/T_2 ratios at or above 5. Interestingly, following pressurized dodecane injection at 5000 psi, T_1/T_2 contrast increased above 10.

A few recent studies were focused on NMR signature of extracted organic matter in different maturity windows (Fleury, 2014; Tinni et al., 2014). Early maturity Woodford shale samples in this study showed that non-movable hydrocarbons remaining in the samples have T_1/T_2 ratios above 30. Original signature of the non-movable hydrocarbons was hidden in the signal of the movable fluids. Multiple samples (3951, 3906) showed two peaks on the T_1-T_2 maps: brine and non-movable hydrocarbons, suggesting that fluid typing is plausible in these rocks. On the contrary, high T_1/T_2 ratio contrast was observed not only in the presence of non-movable hydrocarbons in shales, but also following a pressurized injection of low viscosity oil, such as dodecane.

TMS Results

Laboratory and field CMR-Plus tools were utilized to characterize Tuscaloosa Marine Shale. TMS appears to be strongly water wet, creating capillary blockage and prohibiting hydrocarbon accessibility to the pore network. Residual fluid in the inorganic pores

appears to be brine as indicated by the T_1-T_2 maps. Brine imbibed and "as received" measurements showed that 2.9 p.u., or 40.8% of the total porosity, is filled with irreducible water. Based on laboratory NMR measurements (Figure 40) and SEM images (Figure 15), porosity is contained within the inorganic pores and contribution from the organic porosity is negligible.

Despite the significant production reported by operators, analyses suggest that rock matrix in the TMS does not allow significant hydrocarbon storage. This suggests other storage and production mechanisms are dominant, such as contribution from microfractures or migration of oil from other sources. Resistive vertical fractures captured in the image logs are likely cement filled, while finer scale microfractures are filled with hydrocarbons or oil based mud.

Laboratory NMR porosity and field CMR-Plus porosity are within 2 p.u. of each other. Additionally, the two logging runs showed that formation microfractures can be sensed when CMR-Plus sensor is aligned in the direction of the microfractures.

References

Allen, D., Flaum, C., Ramakrishnan, T., Bedford, J., Castelijns, K., Fairhurst, D., Gubelin, G., Heaton, N., Minh, C.C., Norville M.A., Seim., M.R., Pritchard, T., and Ramamoorthy,. R. 2000. Trends in NMR Logging. *Oilfield Review* 12, no.3, 2-19.

Allen, J.E., Meylan, M.A. and Heitmuller, F.T. 2014. Determining Hydrocarbon Distribution Using Resisitivity, Tuscaloosa Marine Shale, Southwestern Mississippi. Master's Thesis, University of Southern Mississippi, Hattiesburg, Mississippi.

Akkurt, R., Bachman, H.N., Minh, C.C., Flaum, C., LaVigne, J., Leveridge, R., Carmona, R., Crary., S., Decoster, E., Heaton, N., Hurlimann, D., Looyestijn, W.J., Mardon, D., and White, J. 2009. Nuclear Magnetic Resonance Comes Out of Its Shell. Oilfield Rev., v.20,4.

Anand, V., Rampurawala M. A., Al-Adani, N., Willis, D., Freedman, R., Hamichi F., Abubakar, A., Grover, R., Neto, O., Aboud, M., and Iglesias J.G. 2015. New Generation NMR Tool for Robust, Continuous T1 and T2 Measurements. Presented at the 56th SPWLA 56th Annual Logging Symposium**,** *Long* Beach, California, USA, 18–22 July.

Ballard, B. 2007. Quantitative Mineralogy of Reservoir Rocks Using Fourier Transform Infrared Spectroscopy. Paper presented at the SPE Annual Technical Conference and Exhibition, Anaheim, California, USA, 11-14 November.

Bloch, F., Hansen, W.W. and Packard, M. 1946. Nuclear Induction. *Physical Rev*iew v. 69,p.127.

Bohacs, K.M., Passey, Q.R., Rudnicki, M., Esch, W.L., and Lazar, O.R. 2013. The Spectrum of Fine-Grained Reservoir from 'Shale Gas' to 'Shale Oil'/Tight Liquid: Essential Attributes, Key Controls, Practical Characterization. Presented at International Petroleum Technology Conference, 26-28 March, Beijing, China.

Bloembergen, N., Purcell E.M., and Pound, R.V. 1948. Relaxation Effects in Nuclear Magnetic Resonance Absorption. J. *Physical Review*, 73: p. 679-712.

Blumich, B. 2005. *Essential NMR*. Berlin : Springer.

Blumich B., Haber-Pohlmeier S., and Zia W. 2014. *Compact NMR,* first edition. Berlin: De Gruyter.

Cardott, B.J. 2001. Thermal Maturation of the Woodford Shale in Eastern Oklahoma. Oklahoma Geological Survey, Circular 106, p. 193.

Cardott, B.J. 2012. Thermal Maturity of Woodford Shale Gas and Oil Plays, Oklahoma, USA: International Journal of Coal Geology, v. 103, p. 109-119.

Cardott, B.J. 2013. Hartshorne Coal Rank Applied to Arkoma Basin Coalbed Methane Activity, Oklahoma, USA: International Journal of Coal Geology, v. 108, p. 35–46.

Coates, G., Xiao, L., and Prammer, M. 1999. *NMR Logging: Principles and Applications*. Houston: Gulf Publishing Company.

Curtis, M.E., Cardott B.J., Sondergeld, C.H. and Rai, C.S. 2012. The Development of Organic Porosity in the Woodford Shale Related to Thermal Maturity. Presented at the SPE Annual Technical Conference and Exhibition, San Antonio, Texas, 8-10 October.

DePavia, L., Heaton, N., Ayers, D., Freedman, R., Harris, R., Jorion, B., Kovats, J., Luong, B., Rajan, N., Taherian, R., Walter, K. and Willis, D. 2003. A Next-Generation Wireline NMR Logging Tool. Paper presented at the SPE Annual Technical Conference and Exhibition, Denver, 5-8 October.

Dolinsek, J., Vilfan, M. and Zumer, S. 2006. *Novel NMR and EPR Techniques*, first edition.New York: Springer.

Echols, J. B. 1997. Geochemical Analyses of Tuscaloosa Oils. Louisiana State University Basin Research Institute Bulletin,v. 7, p. 23–24.

Fleury, M., Kohler, E., Norrant, F., Gautier, S., M'Hamdi, J., and Barré, L. 2013. Characterization and Quantification of Water in Smectites with Low-Field NMR. *J. Phys. Chem*. C;117:4551–60.

Fleury, M. 2014. Characterization of Shales with Low Field NMR. Paper presented at the International Symposium of the Society of Core Analysts, Avignon, France, 8-11 September.

Freedman, R., Boyd, A., Gubelin, G., McKeon, D., and Morriss, C.E. 1997. Measurement of Total NMR Porosity Adds New Value to NMR Logging. Presented at the SPWLA Annual Logging Symposium, Houston, 15–18 June.

Freedman R. and Morriss C.E. 1998. Processing of Data from an NMR Logging Tool. Presented at the SPE Annual Techinal Conference and Exhibition, 22-25 October.

Green Imaging Technologies. 2014. GIT Systems and LithoMetrix User Manual.

Guo, Y., Zhang, K., and Marfurt, K. 2010. Seismic Attribute Illumination of Woodford Shale Faults and Fractures, Arkoma Basin, OK. Presented at the 80th Annual International SEG Meeting, Expanded Abstracts, 29, 1372–1375.Hahn E.L. 1950. Spin Echoes. *Physical Review*, v.80, 580-594.

Hirasaki, G.J., Lo, S.W., and Zhang, Y. 2003. NMR Properties of Petroleum Reservoir Fluids. Magnetic Resonance Imaging, No. 3–4, 269.

Hook, P., Fairhurst D.L., Rylander, E.I., Badry, R., Bachman, N., Crary, S., Chatawanich, K., and Taylor, T. 2011. Improved Precision Magnetic Resonance Acquisition: Application to Shale Evaluation. Paper presented at the SPE Annual Technical Conference and Exhibition, Denver, 30 October – 2 November.

Houseknecht, D. W., Rouse,W. A., Paxton S. T., Mars, J.C. and Fulk, B. 2014. Upper Devonian–Mississippian Stratigraphic Framework of the Arkoma Basin and Distribution of Potential Source-Rock Facies in the Woodford–Chattanooga and Fayetteville–Caney Shale-Gas Systems. AAPG Bulletin, v. 98, p. 1739-1759.

Houseknecht, D. W., L. A. Hathon, and T. A. McGilvery. 1992. Thermal Maturity of Paleozoic Strata in the Arkoma Basin. Oklahoma Geological Survey, Circular 93, p. 122–132.

Houseknecht, D. W., and S. M. Matthews. 1985. Thermal Maturity of Carboniferous strata, Ouachita Mountains: AAPG Bulletin, v. 69, p. 335–345.

Howe, H.J. 1962. Subsurface Geology of St. Helena, Tangipahoa, Washington and St. Tammany Parishes, Louisiana. Gulf Coast Association of Geological Societies Transactions, v. 12, p. 121-155.

Jarvie, D. M., B. L. Claxton, F. Henk, and J. T. Breyer. 2001. Oil and Shale Gas from the Barnett Shale, Fort Worth Basin, Texas. Presented at the AAPG Annual Meeting, v. 10, p. A100.

John, C.J., Jones B.L, Moncrief, J. E., Bourgeois, R. and Harder, B.J. 1997. An UnprovenUnconventional Seven Billion Barrel Oil Resource - the Tuscaloosa Marine Shale. LSU Basin Research Institute Bulletin. vol. 7, p. 1-22.

John, C.J., Jones, B.L., Harder, B.J., and Bourgeois, R.J. 2005. Exploratory Progress Towards Proving the Billion Barrel Potential of the Tuscaloosa Marine Shale: Gulf Coast Association of Geological Societies Transactions, v. 55, p. 367–372.

Johnson, K.S. 1988. Geologic Evolution of the Anadarko Basin. Anadarko Basin Symposium: Circular 90, Oklahoma Geological Survey, p. 3-12.

Kausik, R., Minh, C., Zielinski, Vissapragada, B., Akkurt, R., Song, Y., Liu, C., Jones, S., and Blair, E. 2011. Characterization of Gas Dynamics in Kerogen Nanopores by NMR. Presented at the SPE Annual Technical Conference and Exhibition, Denver, Colorado, 30 October – 2 November.

Keating, K. and Knight, R. 2009. A Laboratory Study of the Effect of the Fe(II)-Bearing Minerals on Nuclear Magnetic Resonance (NMR) Relaxation Measurements. *Geophysics*, v.75, p.F71-F82.

Kenyon, W.E. 1992. Nuclear Magnetic Resonance as a Petrophysical Measurement. Nuclear Geophys, pp. 153 - 171.

Kleinberg, R.L., Straley C., Kenyon W.E., Akkurt, R., and Farooqui, S.A. 1993. Nuclear Magnetic Resonance of Rocks: T_1 vs. T_2. Presented at the 68th Annual Technical Conference and Exchibibtion of SPE, Houston, Texas, 3-6 October.

Kleinberg, R.L. 1999. Nuclear Magnetic Resonance. *Methods in the Physics of Porous Media*, v. 35, p. 337–385.

Kleinberg R. L. and Jackson J.A. 2001. An Introduction to the History of NMR Well Logging. *Concepts in Magnetic Resonance*, v.12, pp. 340-342.

Lu, J., Ruppel, S. and Rowe, H. 2015. Organic Matter Pores and Oil Generation in the Tuscaloosa Marine Shale. AAPG Bulletin v. 99, p. 333-357.

Mancini, E.A., Mink, R.M., Payton, J.M., and Bearden, B.L. 1987. Environments of Deposition and Petroleum Geology of Tuscaloosa Group (Upper Cretaceous), South Carlton and Pollard fields, Southwestern Alabama: AAPG Bulletin, v. 71, p. 1128–1142.

Mancini, E. A. and Puckett, T. M. 2005. Jurassic and Cretaceous Transgressive-Regressive (T-R) Cycles, Northern Gulf of Mexico, USA: Stratigraphy, v. 2, p. 31–48.

McKeon D., Minh C.C., Freedman R., Harris, R., Willis, D., Davies, D., Gubelin, G., Oldigs, R., and Hurlimann, M. 1999. An Improved NMR Tool Design for Faster Logging. Paper Presented at the SPWLA 40th Annual Logging Symposium.

Menger, S., Prammer, M.G., and Drack, E.D. 1999. Calculation of Combined T1/T2 Spectra from NMR Logging Data. Presented at the 40th Logging SPWLA Symposium.

Molinares, C.E., and Slatt, R.M. 2014. Thomas Amsden's Pre-Woodford Subcrop Maps and the Late Devonian-Early Mississippian Unconventional Plays in the Arkoma Basin: Shale Shaker, v. 65, p. 212-219.

MR Explorer Brochure. 2016a. http://www.bakerhughes.com/news-and-media/resources/brochures/mr-explorer-light-oil-flyer (accessed July 12, 2016).

MR Explorer Brochure. 2016b. http://www.bakerhughes.com/news-and media/resources/brochures/mr-explorer-flyer (accessed July 12, 2016).

Nicot, B., Vorapalawut, N., Rousseau B., Madariaga, L.F., Hamon, G., and Korb, J.P. 2016. Estimating Saturations in Organic Shales Using 2D NMR. *Petrophysics*, v.57, p. 19-29.

Odusina, E., Sondergeld, C.H. and Rai, C. S. 2011. An NMR Study on Shale Wettability. Presented at the Canadian Unconventional Resources Conference, Calgary, Alberta, Canada, 30 October-1 November.

Ostroff, G.M., Shorey, D.S., and Georgi D.T. 1999. Integration of NMR and Conventional Log Data for Improved Petrophysical Evaluation of Shaly Sands. Presented at the 40th SPWLA Logging Symposium, 30 May - 3 June.

Ozen A.E. and Sigal R.F. 2013. T1/T2 NMR Surface Relaxation Ratio for Hydrocarbons and Brines in Contact with Mature Organic-Shale Reservoir Rocks. *Petrophysics*, 54 no. 1, p. 11-19

Prammer, M. 2000. Eccentric NMR Well Logging Apparatus and Method. Export Citation, assignee. Patent US6023164 A.

Purcell, E.M., Torrey, H.C. and Pound, R.V. 1946. Resonance Absorption by Nuclear Moments in a Solid. *Phys. Rev.* v.69, p.37-38.

Reeves, P.C. and Celia M.A. 1996. A Functional Relationship Between Capillary Pressure, Saturation, and Interfacial Area as Revealed by a Pore-Scale Network Model. *Water Resources Research,* v.32, p. 2345-2358.

Saidian, M. 2015. Effect of Rock Composition and Texture on Pore Size Distributions in Shales: Applications in Low Field Nuclear Magnetic Resonance. MS thesis, Colorado School of Mines, Colorado.

Sanchez Energy. 2015. Corporate Presentation. http://www.theoilandgasconference. com/downloads_TOGC_2015/Sanchez-Energy.pdf

Sigal, R.F and Odusina, E. 2011. Laboratory NMR Measurements on Methane Saturated Barnett Shale Samples. Petrophysics 52 (1) (2011)

Sondergeld, C.H. and Rai, C.S. 1993. New Exploration Tool: Quantitative Core Characterization. PAGEOPH, 141, p. 249-268.

Sulucarnain, I., Sondergeld, C.H., and Rai, C.S. 2012. An NMR study of Shale Wettability and Effective Surface Relaxivity. Presented at the Canadian Unconventional Resources Conference, Calgary, Alberta, Canada, 30 October–1 November.

Schon, J.H. 2004. *Physical Properties of Rocks: Fundamentals and Principles of Petrophysics,* first edition. Oxford: Pergamon.

Timur, A. 1969. Pulsed Nuclear Magnetic Resonance Studies of Porosity, Movable Fluid, and Permeability of Sandstones. Journal of Petroleum Technology. 21, 775-786 (1969).

Tinni, A., Sondergeld, C.H., and Rai, C.S. 2014. NMR T_1-T_2 Response of Moveable and Non- Moveable Fluids in Conventional and Unconventional Rocks. Paper presented at the International Symposium of the Society of Core Analysts, 8-11 September, Avignon, France.

Tinni, A., Odusina, E., Sulucarnain, I., Sondergeld, C., and Rai, C.S. 2015. Nuclear_Magnetic-Resonanse Response of Brine, Oil, and Methane in Organic-Rich Shales. *SPE Reservoir Evaluation & Engineering.*

Viele, G.W., and Thomas, W.A. 1989. Tectonic Synthesis of the Ouachita Orogenic Belt. *In* Hatcher, R.D., Jr., Thomas, W.A., and Viele, G.W. *The Appalachian-Ouachita Orogen in the United States*, p. 695–728.

Appendix A: T_2 Distributions of TMS Samples in Various Saturation States

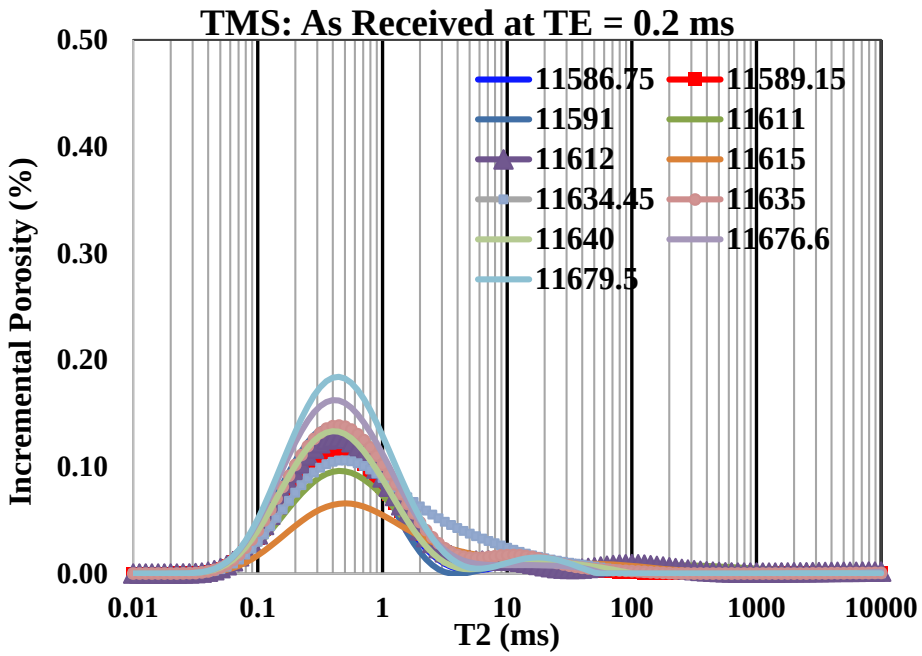

Figure A- 1— T_2 distributions of the TMS samples in the "as received" state.

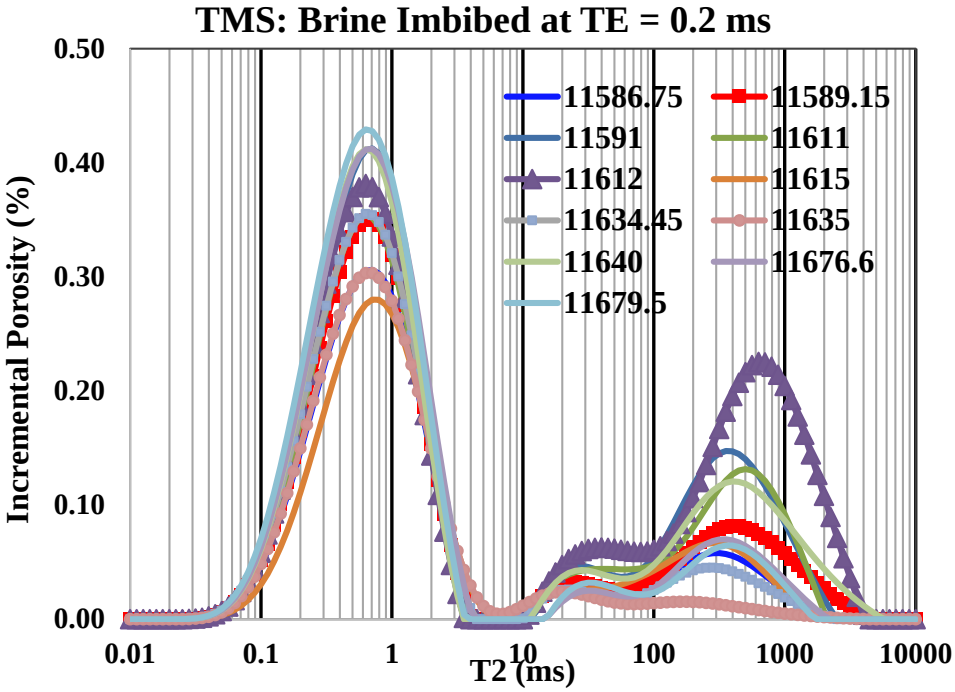

Figure A- 2 — T_2 distributions of the brine imbibed TMS samples

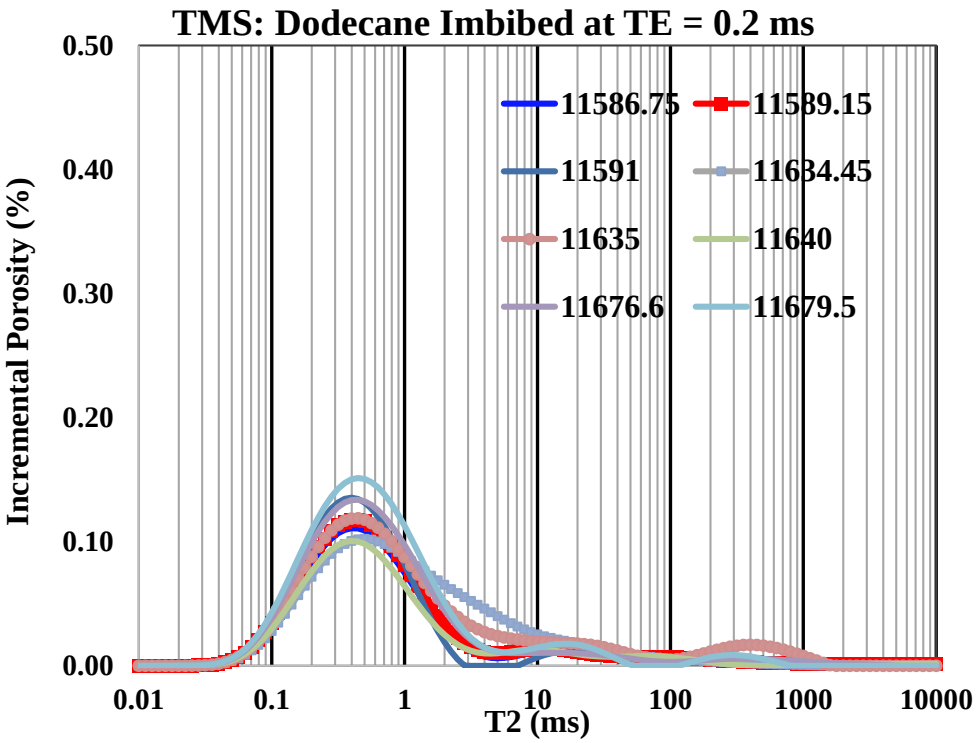

Figure A- 3—T2 distributions of the dodecane imbibed TMS samples

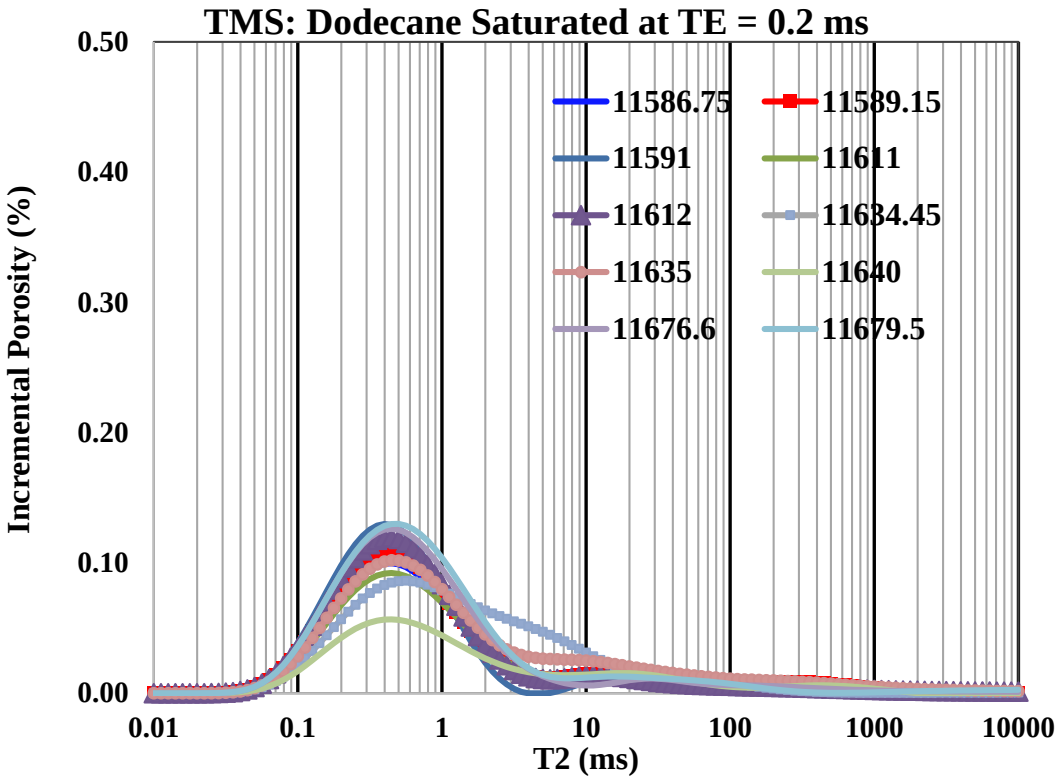

Figure A- 4— T2 distributions of the dodecane saturated TMS samples

Appendix B: T_2 Distributions of Woodford Samples in Various Saturation States

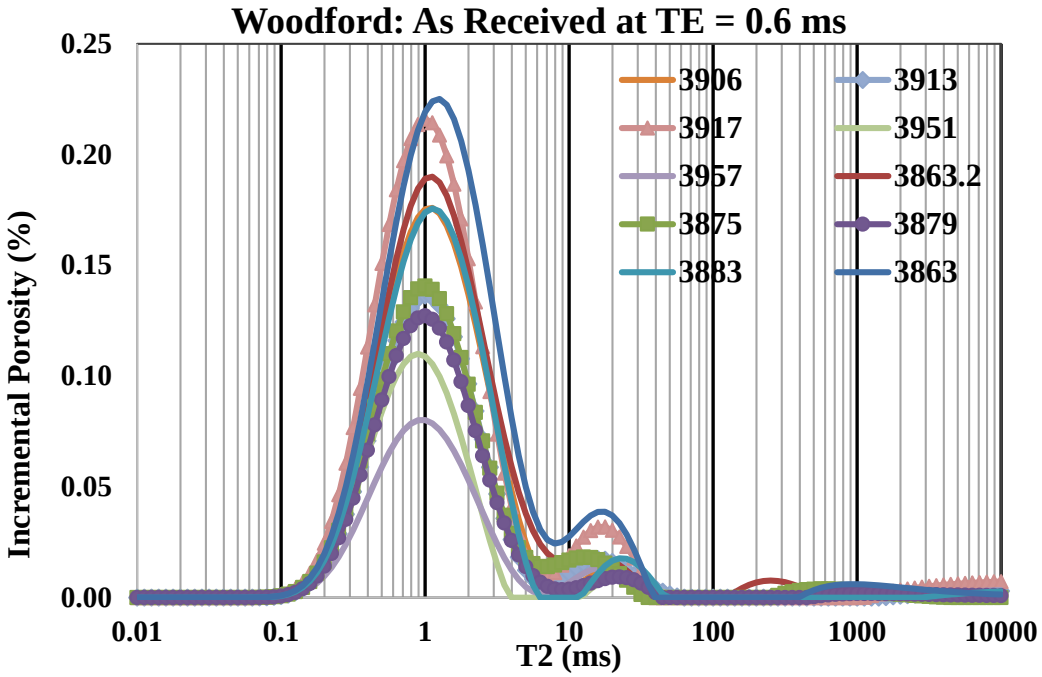

Figure B- 1— T_2 distributions of the Woodford samples in the "as received" state.

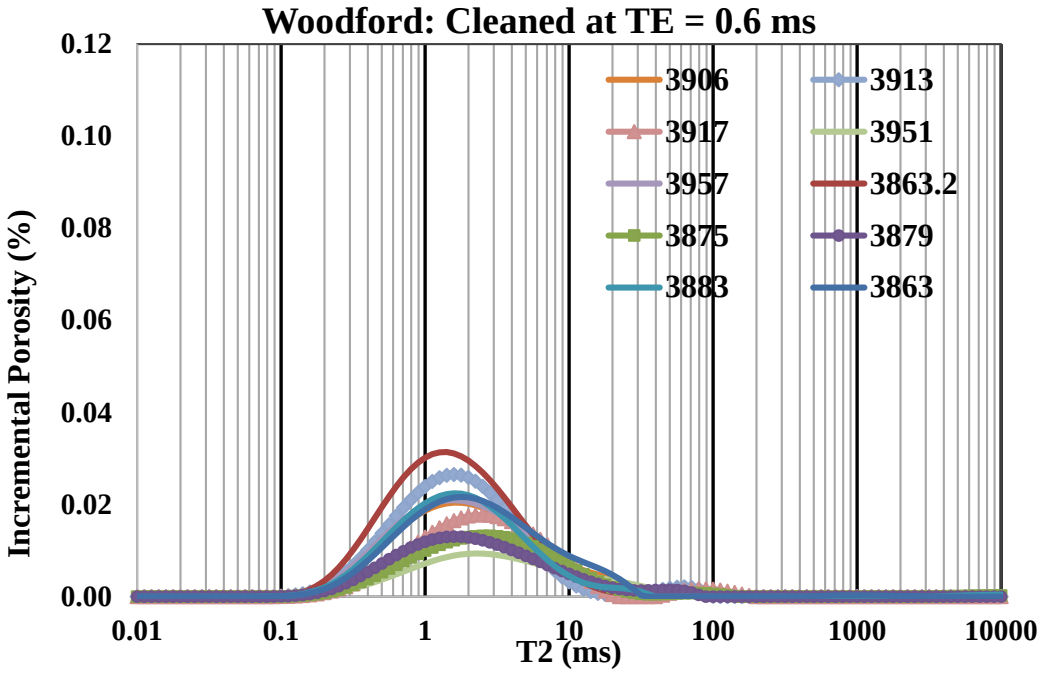

Figure B- 2— T_2 distributions of the cleaned Woodford samples.

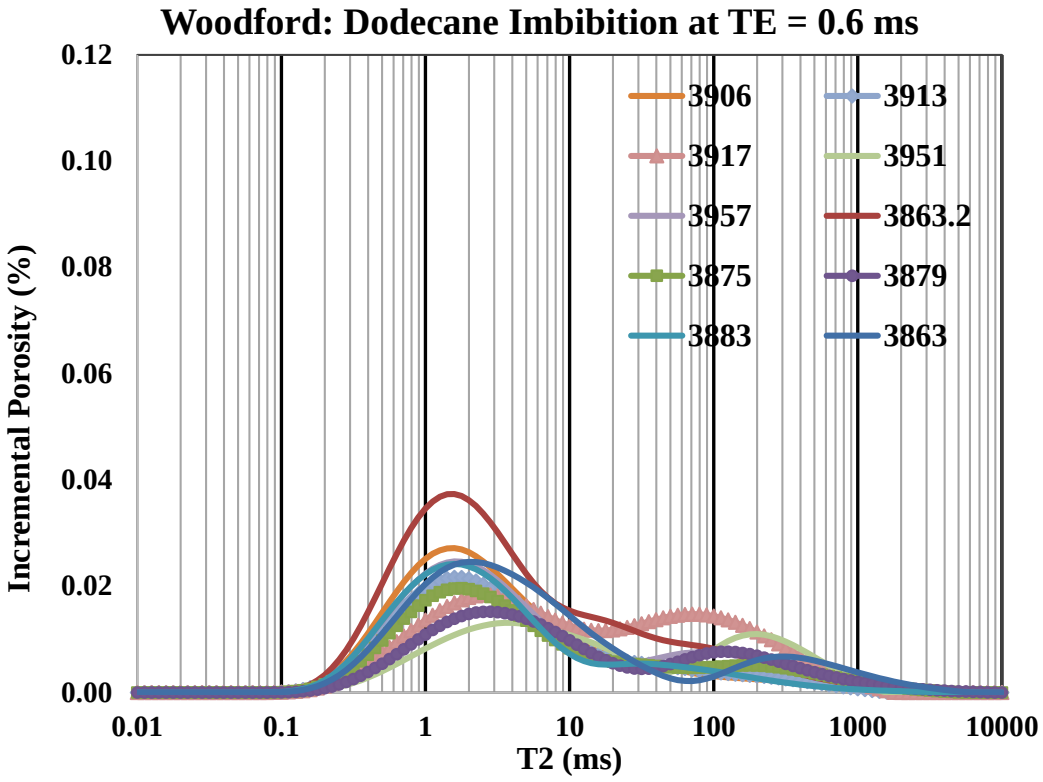

Figure B- 3— T_2 distributions of the dodecane imbibed Woodford samples.

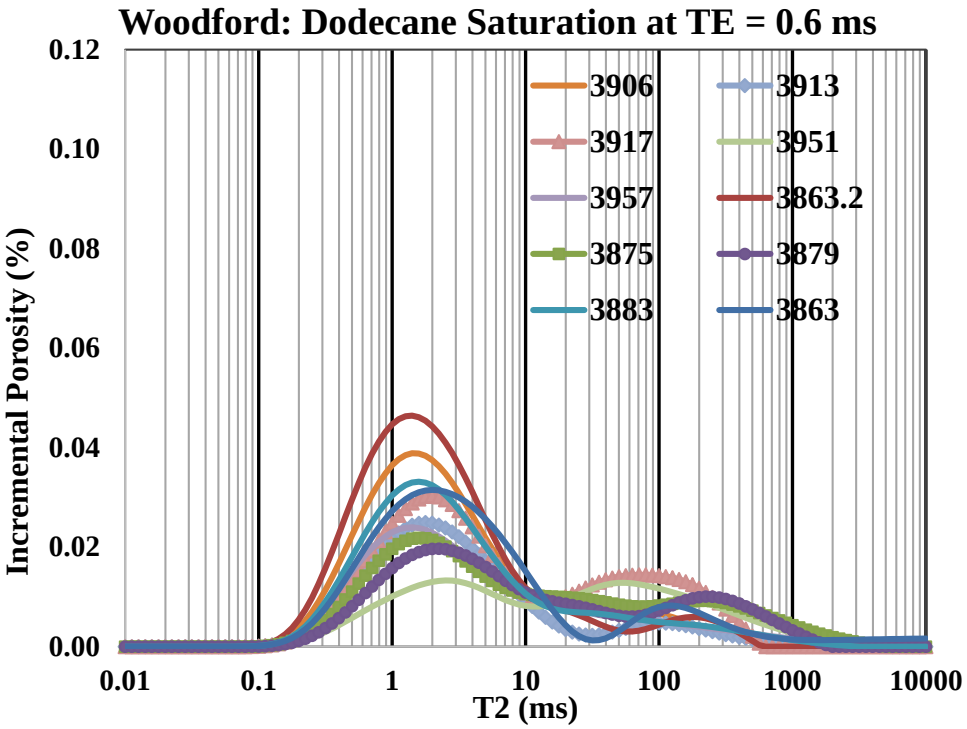

Figure B- 4—T_2 distributions of the dodecane imbibed Woodford samples

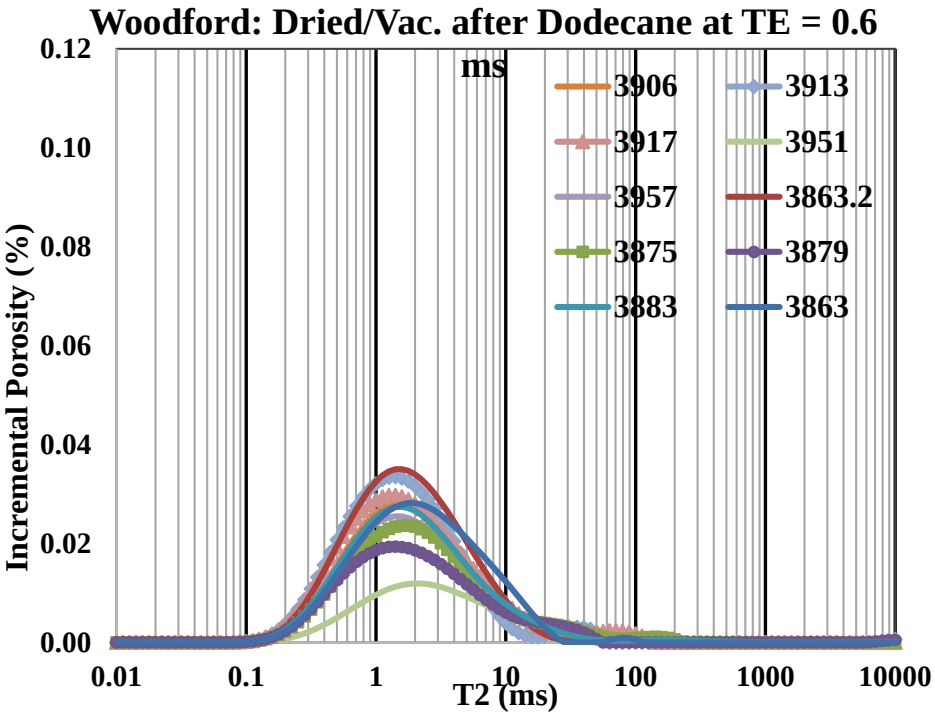

Figure B- 5—T_2 distributions of the dried and vacuumed Woodford samples.

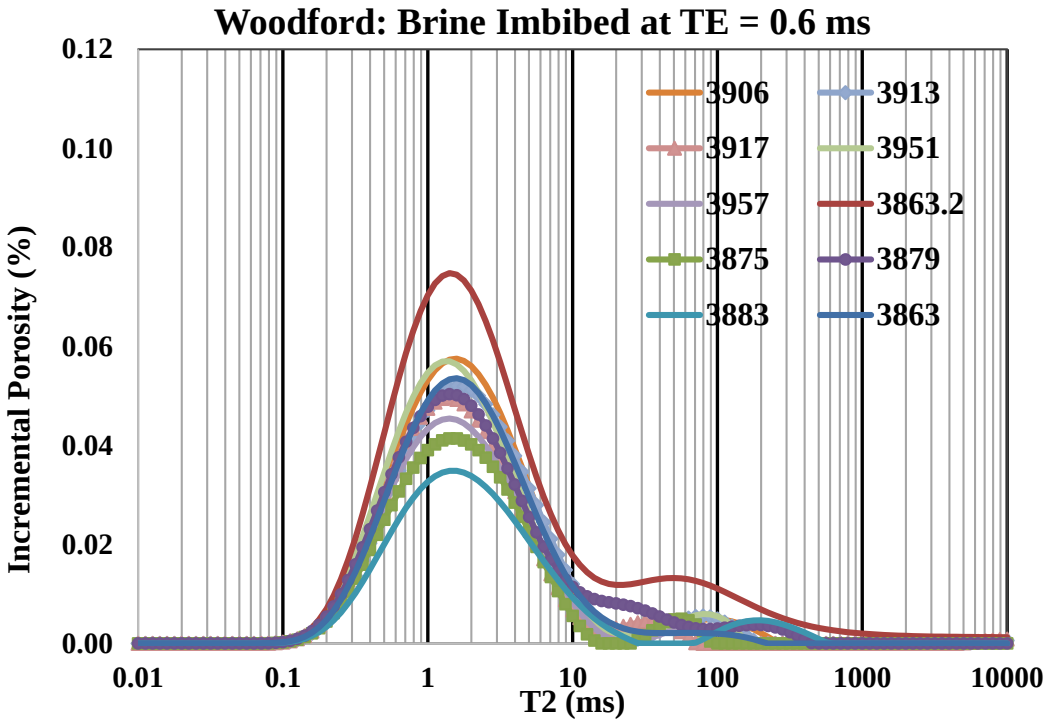

Figure B- 6— T_2 distributions of the brine imbibed Woodford samples.

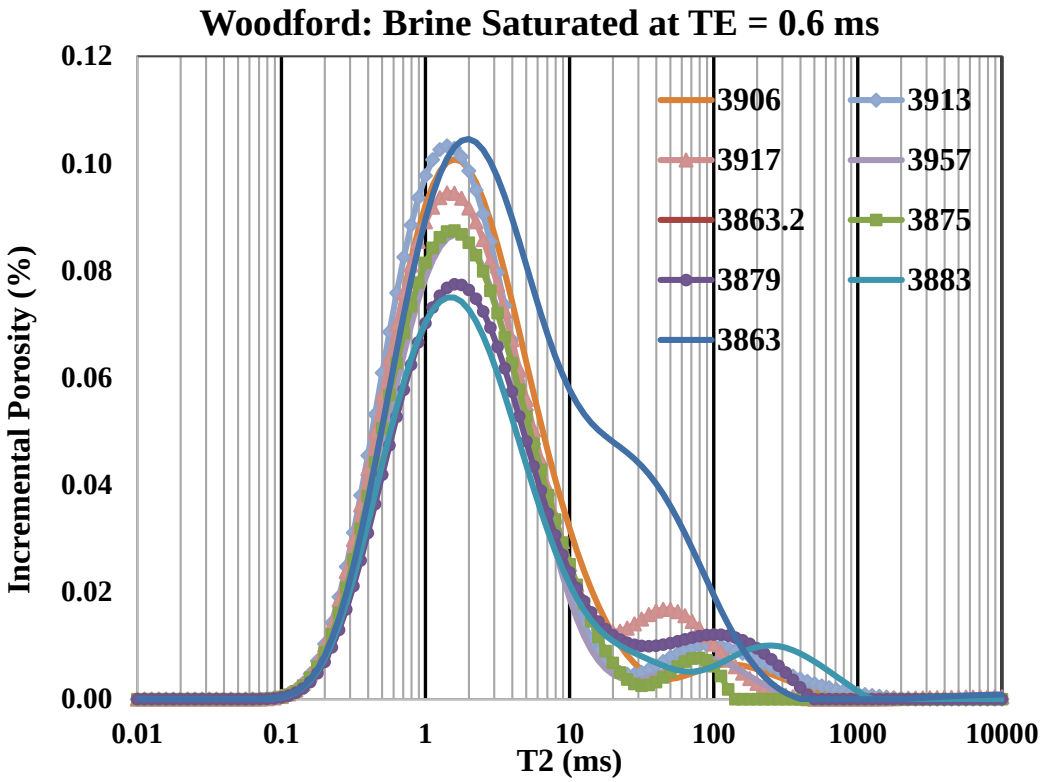

Figure B- 7— T_2 distributions of the brine saturated Woodford samples.